Journal of Rheology

RESEARCH ARTICLE | APRIL 29 2026

A semimicroscopic model to describe nonmonotonic stress relaxation of associative polymer networks

W. J. Briels ; J. K. G. Dhont

J. Rheol. 70, 737–754 (2026)
https://doi.org/10.1122/8.0001120

A semimicroscopic model to describe nonmonotonic stress relaxation of associative polymer networks

W. J. Briels[1,2,a)] and J. K. G. Dhont[1,3,a)]

[1]*Forschungszentrum Juelich, Biomacromolecular Systems and Processes (IBI-4), Wilhelm-Johnen-Strasse, 52428 Juelich, Germany*
[2]*Computational Chemical Physics, University of Twente, P.O. Box 217, 7500 AE Enschede, The Netherlands*
[3]*Department of Physics, Heinrich Heine Universitaet, Universitaetsstrasse, 40225 Düsseldorf, Germany*

(Received 16 September 2025; final revision received 2 March 2026; published 29 April 2026)

Abstract

Recent experiments on associative polymer networks revealed a nonmonotonic stress relaxation after cessation of preshear. A temporal increase in the stress at intermediate times is observed before full relaxation of the stress occurs. Motivated by what is expected to occur on a molecular level, we propose equations of motion for the network stress and the concentration of cross-links. These equations lead to an explicit expression for the time dependence of the stress, which quantitatively reproduces experimental nonmonotonic stress relaxation curves for two different types of associative polymer systems. Our mathematical model involves a time scale for the recovery of cross-links, a Maxwell-type time scale for the final stress relaxation, for the relative number of cross-links that survives the preshear period, and the initial stress right after cessation of preshear. The numerical results for these parameters obtained from the comparison with experiments allow for a further interpretation of the underlying mechanisms on a molecular level depending on the type of associative polymer. https://doi.org/10.1122/8.0001120

I. INTRODUCTION

It is a common experience that stresses built up during shearing of a viscoelastic system decay monotonously after shearing has been stopped. It, therefore, came as a surprise when with a slightly entangled EHUT system [an organo gel consisting of stacked 2, 4-bis (2-ethyl-hexyl-ureido) toluene molecules dissolved in dodecane; further information in Sec. III C], in some cases, an initially decaying stress after a while started to move up again and only much later began to decay again to reach a state of zero stress, often after as much as several minutes [1].[1] In order to be convinced that it was not an experimental artifact being measured, several more systems were subsequently investigated until, in total, three systems were found showing this remarkable phenomenon. The results were published in a paper by Hendriks *et al.* [2].

In addition to the EHUT system, two polymeric systems have been studied in [2]: one, in which polymers are dressed with ligands which can mutually bind, and the other, where ligand–ion–ligand bonds are formed. As a result, both systems form a network with gel-like properties. A rough understanding of the phenomenon then goes as follows: during shearing, bonds are broken by which energy is stored in the system, and molecules are disentangled and aligned, by which entropy is removed from the system. In total, the free energy of the system is raised. After cessation of the shearing motion, the system relaxes to the initial state of lower free energy by re-establishing bonds and thermally randomizing its molecules.

It is important to realize that bond formation itself, leading to a decrease in the internal energy, has hardly any effect on the stress of the system, and that the latter is mainly resulting from polymeric, i.e., entropic springs, and how they are constrained by cross-linking bonds. Moreover, even though the free energy decreases monotonously to its minimum value, the constituents, energy and entropy need not do so. As a result, stresses, being a measure of the entropy, can relax nonmonotonously [2,3]. It is our intention in this paper to develop a semimicroscopic model to describe nonmonotonous stress relaxation along these lines.

The theoretical model that we propose applies to associative polymers, where by definition, cross-linking bonds are sufficiently weak to occasionally break by thermal agitation and externally applied stresses. The cross-linking bonds in such systems of associative polymers, for example, can be of a hydrophobic or electrostatic nature. Moreover, instead of molecular polymeric chains, the chains may be supramolecular, where monomers are stacked to form long flexible tubes.

During the last few years, several other systems have been found that show stress-upswings after removing an initial constant preshear rate, either completely or partially. We restrict ourselves to mention carbon-black suspensions [4], fumed-silica dispersions [5], and boehmite gels [6]. In

[a)]Authors to whom correspondence should be addressed; electronic email: w.j.briels@utwente.nl and j.k.g.dhont@fz-juelich.de

[1]Also, presented in a lecture by Louhichi A., A. R. Jacob, J. L. Bouteiller, and D. Vlassopoulos, Nonlinear shear rheology of a supramolecular organogelator, in *The Society of Rheology 87th Annual Meeting*, Baltimore, MD, 11–15 October 2015 (The Society of Rheology, Melville, NY, 2015)

particular, in the last reference, a thorough investigation was done to classify different possible regimes with different behaviors.

Even when it will turn out that one and the same phenomenology will be able to describe the behavior of all these systems, the molecular interpretation of relations between the various parameters of the model can be very different in different cases. We here restrict ourselves, therefore, to associating polymer networks and related systems. In a special section (Sec. III), we will compare our theoretical approach with a few other approaches published recently.

The paper is structured as follows. In Sec. II, we describe our approach and final equations. First, in Subsection II A, we describe the molecular picture that we have in mind to guide us through the rest of the section. Next, in Subsection II B, we develop the rheological model that forms the core of our paper. In a nutshell, we write the stress as the sum of an initial, fast relaxing Rouse-like elastic contribution right after cessation of the preshear, during which cross-links are supposed to remain intact, and the remaining cross-link network contribution. The latter contribution gives rise to the stress upswing. It is the product of a time dependent system strain and a time-dependent shear modulus, for both of which we write down equations of motion. In Subsection II C, we solve the mathematical model just presented, and next discuss some of its characteristics in Subsection II D. In Subsection II E, we describe how, in general, some or all parameters that figure in our theory can be estimated on the basis of a few characteristic features of the experimental data. This section is particularly interesting for experimentalists who do not want to produce full fits of our theory to their data. In Sec. III, we present our fits to experimental data for the three different associating fluids that also have been discussed in [2]. Also, we discuss some trends in the variations of parameters among different, but similar, systems and shear rates, and how they are related to molecular structures. We continue in Sec. IV with a note on a possible relation between the occurrence of stress upswings and shear banding in systems considered in this paper. In Sec. V, we give a short comparison of our theory with other theories suggested in the literature until now. We end with a summary and some conclusions.

II. STRESS RELAXATION FOR ASSOCIATIVE POLYMERS

As discussed in Sec. I, it is our intention to develop a model that captures the essential physics that is responsible for the stress upswings and, at the same time, is sufficiently general to be applicable to a broad class of associative polymers. When developing the model, we will use the language of associating polymers, much in the spirit as presented in the papers of Tanaka and Edwards on the rheological properties of such systems [7,8].

A. The molecular picture

First of all, we will assume that at the time when the shear is stopped, to be called time zero, there are still enough cross-links intact in order that the network is still space filling. Immediately after cessation of the externally applied shear, the flow velocity will relax to zero in a very short time. Subsequently, chains which are severely stretched will relax in an elastic, Rouse-like fashion until this relaxation is halted by constraints set by the distribution of cross-links. This relaxation takes place on a time scale that is usually less than 0.1% of the time needed for the system to reach its final equilibrium state and, so far, has never been resolved experimentally in detail. Here, we will refrain from describing this part of the stress relaxation process in detail and describe it by a single exponential decay. As will turn out in Sec. III, this describes the experiments remarkably well except in one case in Sec. III B where the deviations can be attributed to the molecular structure of that particular system. Our main concern, however, will be the unexpected stress increase and subsequent final relaxation.

The distribution of cross-links has been perturbed during the shearing motion before time zero and after the initial Rouse retraction relaxes to its equilibrium distribution corresponding to minimal free energy. In order to do so, additional bonds must be formed and existing bonds must be broken and re-established to allow further relaxation of chains under tension. In general, this is a slow process as compared to the above-mentioned initial Rouse-like stress relaxation.

When developing a model to describe the cross-link relaxation, we will make the following assumptions. First, bonds are, in general, between two or at most a few functionalized groups. Bonds are strong in the sense that bond breaking is rare. When two functionalized groups meet, a bond will quickly be formed with very high probability. As a consequence of this, in the final equilibrium state, almost all possible bonds will be formed and the number of bonds will slowly fluctuate around its average value.

As a second assumption, the number of functionalized groups is assumed to be small as compared to the number of chain segments. Typically, the number of polymer segments between two functionalized groups is about 20. This implies that an unbound functionalized group will at best find a single or at most a few neighboring unbounded functional group to form a cross-link, on time scales small compared to the relaxation dynamics of the polymer network but large compared to the initial elastic relaxation. Incidentally, this allows us to consider the strands between two cross-links to behave like Rouse chains when providing qualitative arguments to motivate particular assumptions made along the way.

A third assumption is that entanglement stresses and stresses due to dangling ends and loops are not dominant. This requires that the entanglement length is larger than the typical length of the elastically active chains, which are bound on both sides by cross-links.

Before embarking on the details of the mathematical model, let us quickly mention its basic ingredients. There are obviously at least two molecular descriptors needed to describe the rheological response of the network. One is the number concentration of cross-links $c(t)$ and the other is the deformation of the network as quantified by the system strain $\gamma(t)$, both depending on time. Of these, the definition of the network strain may need some clarification. In a nonsheared system, the average values of the coordinate differences, ΔX,

ΔY, and ΔZ, of two adjacent cross-links will be zero. In a sheared system, one of them, say $\langle \Delta Z \rangle$, will be still zero while the others are related by $\langle \Delta X \rangle = \gamma \langle \Delta Y \rangle$, with γ being the strain of the network. This is a characteristic of the mechanical state of the system. It is, for viscoelastic materials, not related in an easy way to the imposed external strain, as found by integrating the external strain-rate over time.

B. The mathematical model

As discussed above, from time zero on the stress in the system quickly relaxes in a Rouse-like manner until it is halted by the distribution of cross-links. The remaining stress relaxes on a time scale much longer than that of all Rouse relaxations in the system. The total stress σ_{tot} is, therefore, written as

$$\sigma_{tot}(t) = \sigma_e(t) + \sigma(t), \tag{1}$$

with

$$\sigma_e(t) = \sigma_{0,e} \exp\left\{-\frac{t}{\tau_e}\right\} \tag{2}$$

being the elastic Rouse-like stress and σ being the remaining physical network cross-link stress. Here, $\sigma_{0,e}$ is the initial elastic stress right after cessation of the externally applied shear and the accompanied flow, and τ_e is the elastic relaxation time. For clarity, we mention that all of σ_{tot} is of elastic origin (we consider the solvent contribution to the stress to be negligible). The initial stress relaxation $\sigma_e(t)$ represents the stress that relaxes by retraction of severely elongated polymers. These may be freely floating polymers and dangling strands that relax through Rouse relaxation, or internal network strands that relax through Rouse relaxation by small displacements of the cross-links as far as this is allowed by the connectivity and boundary conditions. The remaining stress can only relax through bond breaking and bond reformation. This is the stress that we call network stress, σ, for which we next develop a generic model. While doing so, we will assume that after the initial relaxation the strain is small enough to restrict the model to lowest order in strain. Further information about this point will be given at appropriate places in this section.

As mentioned in Sec. II A, the rheological state of the system is determined by the cross-link density and the system strain. These are the two independent variables of our model. With this assumption, the stress becomes a time local property of these two variables. We, therefore, write

$$\sigma(t) = G(t)\gamma(t), \tag{3}$$

where the shear modulus G is taken to be independent of the strain. G does vary with time, however, because the cross-link properties of the network are varying with time. We, thus, assume a linear elastic response of the network. The maximum allowed strain to meet this criterion depends on the molecular structure of the network. In particular, this requires that the distance between two neighboring cross-links is much smaller than the contour length of the corresponding strand.

We emphasize at this point that, like with any coarse description of the system dynamics, the time development of $c(t)$ and $\gamma(t)$ will involve memory integrals. These will next appear in the expression for the stress $\sigma(t)$. Since all memory kernels turn out to be exponential, the corresponding integrals can be carried out and no explicit signs of memory remain.

The network strain γ relaxes because with every bond breaking, either induced by large stresses or thermally, the network relaxes its strain a bit before the free functionalized groups form new bonds. In Appendix A [see Eq. (A8)], it is shown that the probability R_- for a bond to snap per unit of time, to leading order in γ, is given by

$$R_- = K_- + K_- \frac{1}{5}\frac{x_b l_0}{nb^2}\gamma^2 = K_-\left(1 + \frac{1}{5}\frac{x_b l_0}{nb^2}\gamma^2\right), \tag{4}$$

where K_- is a thermal snapping rate depending on temperature and cross-link density [see Eq. (A9)], but not on system strain, while the second contribution is proportional to K_- and strain squared. Here, it is used that the spring constant k of a Rouse chain is equal to $3k_BT/nb^2$. For definiteness, we have given the proportionality factor that applies for Rouse strands between cross-links that are a distance l_0 apart and consist of n Kuhn segments with Kuhn-length b. x_b is the width of the potential well in which two functionalized groups are trapped when forming a bond. The factor in front of γ^2 is smaller than one, so the strain dependence of R_- may be neglected in case γ^2 is less than one.

For the small strains under consideration, we will assume that the amount by which the strain relaxes due to a single bond breakage is proportional to the strain itself, i.e., equal to $s\gamma$. Ignoring the strain induced snapping, as discussed above, the number of bonds that snap per volume and per second becomes cK_- and so the strain will relax according to

$$\frac{d\gamma(t)}{dt} = -cK_- s\ \gamma = -\mathcal{S}\,\sigma(t). \tag{5}$$

With the second equal sign, we have introduced $\mathcal{S} = K_-\, s/\mathcal{A}$, where $\mathcal{A}$ comes from $G = \mathcal{A}\, c$ as will be discussed later in this section. There we will argue that $\mathcal{A}$ is a constant. This leaves us with K_- and s, both of which will be assumed to be constant. The specification of their dependency of cross-link density and/or strain requires a true molecular approach, for example, by means of computer simulations. We are convinced that the essential physics is taken care of by the dependencies already introduced in the above approach. $\mathcal{S} > 0$ will be referred to as the bond-snapping parameter. Note that $d\gamma(t)/dt$ is not associated with flow nor an externally applied shear rate, both of which vanish.

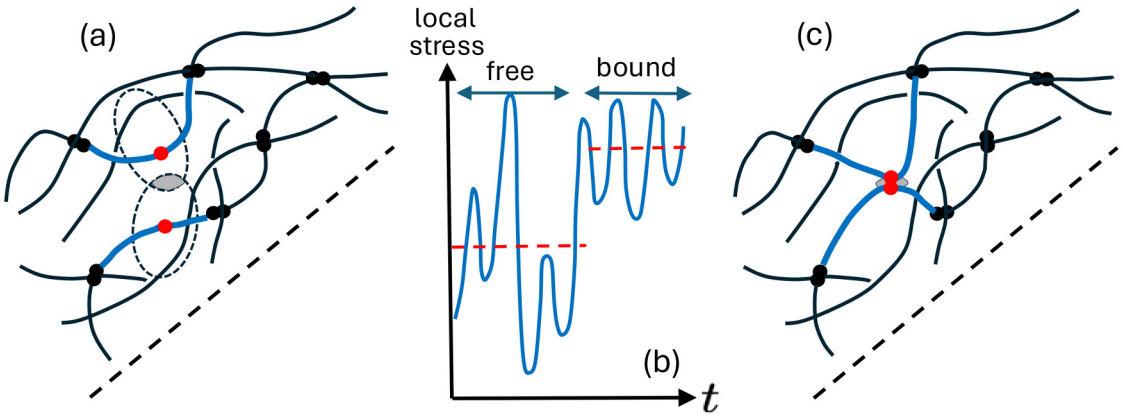

FIG. 1. A cartoon that visualizes bond formation in the strained network. The dotted line indicates the strain direction. (a) The black double dots represent two bound functional groups, which cross-link two polymer chains. The two red dots are free functional groups that can probe a volume indicated by the dashed areas. These volumes are mainly defined by the constraining polymer chains indicated in blue. The two groups can only meet within the overlap of the two volumes, indicated in gray. In (b), the thermally induced local stress fluctuations due to the fluctuating positions of the two free groups is sketched. Once the two free groups simultaneously reside within the overlap volume and are within the range of the attractive interaction potential between the two groups, a bond is immediately formed. The local thermally averaged stress before and after binding is indicated by the red striped lines. The additional stretching of the confining chains in blue, as depicted in (c), leads to an immediate increase in the local stress depicted in (b). The vectorial component of the stretching forces along the shearing direction contributes to the total network stress.

Eliminating $\gamma(t)$ among Eqs. (3) and (5), we get

$$\frac{d\sigma(t)}{dt} = G(t)\frac{d\gamma(t)}{dt} + \frac{dG(t)}{dt}\gamma(t) = -\mathcal{S}\,G(t)\sigma(t) + \frac{d\ln G(t)}{dt}\sigma(t). \tag{6}$$

Before continuing with the general development of the model, we want to discuss basic Eq. (6) a bit further. In particular, we will briefly address the mechanism through which re-establishment of cross-links for a given finite strain gives rise to an increase in the stress, which is formally accounted for by the second terms on the right-hand side of Eq. (6), noting that $dG/dt = (dG/dc)(dc/dt)$. In a strained network, there are more strands that are roughly oriented along the strain direction than along the "orthogonal" direction. The former give a positive contribution to the stress while the others give a negative contribution. Moreover, the "parallel" strands are stretched and, therefore, are under larger tension than the others which are compressed compared to their lengths in equilibrium. Finally, there will be more free groups along the stretched strands than along the compressed strands, and so there will be more cross-links re-established by combining free groups which are both on parallel strands than otherwise. A typical situation is pictured in Fig. 1. A bond between two unbound neighboring functional groups can only occur when the volumes available for the two groups overlap, indicated by the gray area in Fig. 1(a). The two free groups bind once the distance between them is less than the range of the attractive interaction potential between them. As long as the groups are not bound, large volumes are available corresponding to large fluctuations in the stress [Fig. 1(b)]. Configurations where a bond may occur typically correspond to large tensions in the strands. Once a bond is formed [Fig. 1(c)], the two groups are restricted to probe a limited volume, where the stress fluctuates around an average stress that is larger than before bond formation. Typical stress fluctuations are shown in Fig. 1(b).

We now make the argument more quantitative. Consider a network with a given strain γ and a given number of bound groups per unit volume c, and imagine that dc new bonds per unit volume are formed. As discussed before, the initially free groups, and the attached polymer strands, become constrained in their motion upon binding and lose entropy. As depicted in Fig. 1, this leaves the polymer strands involved (indicated in blue) in this process under tension. Due to this single-bond event at the prescribed strain, the stress response of the network is increased by an amount $d\sigma = f\gamma$, where f is a constant. For a number $V\,dc$ of such new bonds, where V is the volume of the system, the stress increase equals $d\sigma = \mathcal{A}\gamma\,dc$, where $\mathcal{A} = fV$. As a consequence, the newly formed bonds lead to an increase $dG = \mathcal{A}\,dc$, in agreement with Eq. (6). Assuming that $\mathcal{A}$ is independent of γ and c, we may write

$$G(t) = \mathcal{A}c(t). \tag{7}$$

In Appendix B1, we will argue that, in general, $\mathcal{A} = ac^{\nu}$ with ν being a small number, positive or negative depending on the precise system under consideration. In this paper, we will take $\mathcal{A}$ to be constant assuming that in important cases, this is accurate enough and thereby extending the applicability of our equations. In Appendix B, it is shown that for strands composed of Rouse chains, $\nu = 1/3$. With c typically ranging from about 0.5 c_∞ to c_∞ (see below), with c_∞ being the cross-link density in equilibrium, $(c/c_\infty)^{1/3}$ varies between 0.8 and 1.0. In order to be able to provide analytical expressions as our final result, we take the error for granted and assume $\nu = 0$. In case finite values of ν must be used, the basic equations that we derive must be solved numerically. The independence of $\mathcal{A}$ from strain, thus assuming linear-elastic network response, has been discussed below Eq. (3).

We now return to Eq. (6). Clearly, as soon as $G(t)$ does not vary with time, any more after bond formation is complete, the stress will relax single exponentially with a time constant,

$$\tau_\infty = \frac{1}{\mathcal{S}\, G_\infty}, \tag{8}$$

where G_∞ is the shear modulus of the network in equilibrium after full relaxation of the stress. With $\mathcal{S}$ and G_∞ being constants, τ_∞ will be constant. The above equation of motion is formally equivalent to the classic Maxwell model with a time-dependent shear modules as already used by Joshi [3]. The physics described by this equation depends on how the shear modulus is related to molecular properties. This is where we differ from the approach of Joshi as will be discussed in Sec. V.

Equation (6) can formally be solved to express the cross-link stress in terms of the shear modulus,

$$\begin{aligned}\frac{\sigma(t)}{\sigma_0} &= \frac{G(t)}{G_0}\exp\left\{-\mathcal{S}\int_0^t dt' G(t')\right\} \\ &= \frac{G(t)}{G_0}\exp\left\{-\frac{1}{\tau_\infty}\int_0^t dt' \frac{G(t')}{G_\infty}\right\},\end{aligned} \tag{9}$$

where $\sigma_0 = \sigma(0)$, $G_0 = G(0)$, and G_∞ is the shear modulus of the equilibrium network, after full relaxation of the stress.

For a full description of the stress in the system, we need a second relation between $G(t)$ and $\sigma(t)$, or just an equation to calculate $G(t)$ as a function of time. As already mentioned, we will do this by considering the consequences of bond breaking and reorganization. We will make use of the relation between $G(t)$ and the number density of bonds $c(t)$ in the system [see Eq. (7)] and next, derive an equation that describes the time evolution of $c(t)$. Combining the two, we obtain a kinetic equation for the shear modulus $G(t)$.

In order to derive a kinetic equation for the time evolution of the bond concentration, we need to know the rates of bond breaking and those of bond formation. The first we have already discussed, so we now concentrate on bond formation. The assumption we make is that unbound functional groups are sufficiently immobilized such that each can bind to at most one or a few neighboring functional groups to form a cross-link, similar to what is depicted in Fig. 1. This requires that the volumes probed by free functional groups are sufficiently small. The more the polymer chains are stretched, the larger is the tension imposed on the polymer chains, and the smaller is the volume probed by functional groups. In such situations, the rate of bond formation is proportional to the number concentration $c_{\max} - c$ of unbound functional groups, where $c_{\max}$ is the maximum possible concentration of cross-links so that

$$\frac{dc(t)}{dt} = K_+[c_{\max} - c(t)] - K_-\, c(t), \tag{10}$$

where K_+ is a reaction rate with the dimension of inverse time. The last term describes the thermal snapping of bonds as in Eq. (4) with the neglect of the term quadratic in γ as motivated before. Just like K_-, we will assume that K_+ is a constant.

It is convenient to define

$$c_\infty = \frac{K_+}{K_+ + K_-}\, c_{\max} =: \tau_b\, K_+\, c_{\max}, \tag{11}$$

which allows us to write

$$\frac{dc(t)}{dt} = \frac{c_\infty - c(t)}{\tau_b}. \tag{12}$$

Clearly, c_∞ is the value taken by the bond number concentration $c(t)$ after it has fully relaxed to its equilibrium stress-free state. The characteristic time τ_b will be referred to as the bond formation time. It is determined by the combined effect of K_+ and K_-, but it is to be expected that K_+ is the largest of the two. As a result, the equilibrium bond density c_∞ will be very close to $c_{\max}$, with the difference

$$c_{\max} - c_\infty = c_{\max}\, \tau_b\, K_-, \tag{13}$$

reflecting the strength of the bonds through the Arrhenius law.

We note that the same linear dependence on $c_{\max} - c(t)$ for the temporal evolution of the number of cross-links has also been proposed, although without further motivation, in [7] and [8], in case of end-functionalized polymers. Moreover, a linear dependence is often assumed for equations of motion for structure parameters [9,10]. In our case, the structure parameter is defined as $\lambda = c/c_\infty$ for which $\lambda = 0$ corresponds to the "fluidized state" and $\lambda = 1$ to the "solid state."

With τ_b, we have introduced our third characteristic time.

Multiplying Eq. (12) by $\mathcal{A}$, we obtain the second relation between stress and shear modulus that we were looking for

$$\frac{dG(t)}{dt} = \frac{G_\infty - G(t)}{\tau_b}. \tag{14}$$

In a stress-free system, $G_\infty = \mathcal{A}\, c_\infty$ is the constant value to which the shear modulus will finally settle.

C. Solution of the model

We must now solve the stress from two Eqs. (6) and (14).

Equation (14) can immediately be integrated, yielding

$$G(t) = G_\infty - (G_\infty - G_0)\exp\left\{-\frac{t}{\tau_b}\right\}. \tag{15}$$

Substitution into Eq. (9) thus leads to

$$\begin{aligned}\frac{\sigma(t)}{\sigma_0} = &\left[1 - \frac{G_\infty - G_0}{G_0}\left(e^{-t/\tau_b} - 1\right)\right] \\ &\times \exp\left\{-\left[\frac{t}{\tau_\infty} + \frac{\tau_b}{\tau_0}\frac{G_\infty - G_0}{G_0}\left(e^{-t/\tau_b} - 1\right)\right]\right\}.\end{aligned} \tag{16}$$

Here, σ_0 is the initial value $\sigma(0)$ for the cross-link stress, i.e., $\sigma_0 = \sigma_{tot}(0) - \sigma_{0,e}$. The characteristic time τ_0 is not a new

independent constant but is related to τ_∞ by

$$\tau_0 = \frac{G_\infty}{G_0}\,\tau_\infty = \frac{1}{\mathcal{S}\,G_0}, \tag{17}$$

with τ_∞ taken from Eq. (8).

The explicit time dependence of the total stress is thus finally found from Eqs. (1), (2), and (16),

$$\frac{\sigma_{tot}(t)}{\sigma_0} = \frac{\sigma_{0,e}}{\sigma_0}\exp\left\{-\frac{t}{\tau_e}\right\} + \left[1 - \frac{G_\infty - G_0}{G_0}\left(e^{-t/\tau_b} - 1\right)\right] \times \exp\left\{-\left[\frac{t}{\tau_\infty} + \frac{\tau_b}{\tau_0}\frac{G_\infty - G_0}{G_0}\left(e^{-t/\tau_b} - 1\right)\right]\right\}. \tag{18}$$

The implications for the time dependence of the stress will be analyzed in Subsection II D.

Let us for clarity recapitulate the various quantities appearing in Eq. (18) for the stress. First of all, there are three time scales: τ_e, which is the exponential decay time of the fast initial Rouse-like relaxation, τ_b is the bond-formation time, and τ_∞ is the final Maxwell-like relaxation time [the time τ_0 is related to τ_∞ by Eq. (17)]. Two initial stresses appear: σ_0 is the initial network stress that remains after the fast Rouse-like relaxation, and $\sigma_{0,e}$ is the initial elastic stress. Finally, G_0 and G_∞ are the initial shear modulus and the modulus of the equilibrium network after full relaxation of the stress. We note that G_0 and G_∞ appear only as their ratio, while the $\sigma_0 + \sigma_{0,e}$ is equal to the stress under stationary shear.

D. Characteristic time scales and numerical examples

According to our final result for the cross-link stress in Eq. (16), at times $t/\tau_b \gg 1$, the decay of the cross-link stress σ is single exponential with the time constant τ_∞ defined in Eq. (8). In case $t/\tau_b \ll 1$, the behavior is more subtle,

$$\frac{\sigma(t)}{\sigma_0} = \left[1 + \frac{G_\infty - G_0}{G_0}\,\frac{t}{\tau_b}\right]e^{-t/\tau_0}. \tag{19}$$

From this, we infer that for times when $t/\tau_0 \ll 1$ as well

$$\frac{\sigma(t)}{\sigma_0} = 1 + \left[\frac{G_\infty - G_0}{G_0} - \frac{\tau_b}{\tau_0}\right]\frac{t}{\tau_b}, \tag{20}$$

and hence that the cross-link stress will initially increase when

$$\frac{\tau_b}{\tau_0} < \frac{G_\infty - G_0}{G_0} \quad \text{or} \quad \frac{\sqrt{\tau_b\tau_\infty}}{\tau_0} < \sqrt{\frac{G_\infty - G_0}{G_\infty}}. \tag{21}$$

Only if this condition is met, an upswing of the stress can occur. It is interesting to notice that the fraction on the right-hand side in the second version is equal to the fraction of bonds occurring in equilibrium that has been broken by preshearing; so, the geometric mean of τ_b and τ_∞ divided by τ_0 must be less than the square root of the fraction of bonds broken during the preshear stage.

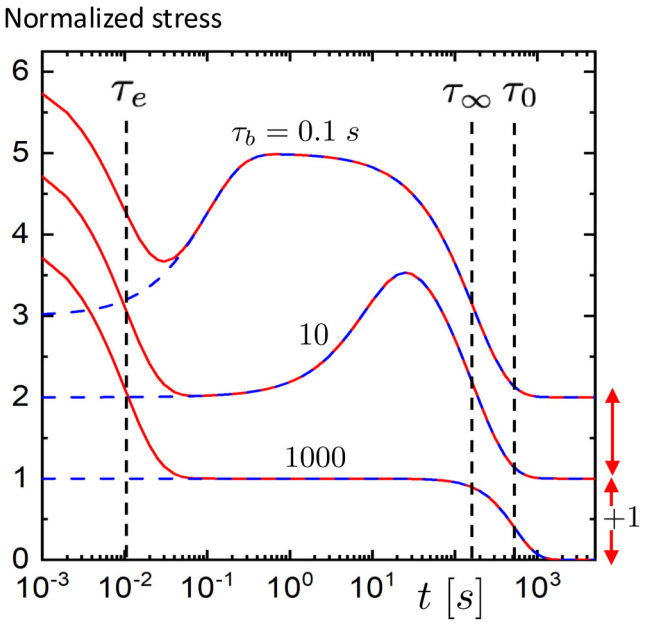

FIG. 2. The normalized cross-link stress σ/σ_0 [the blue dashed line; see Eq. (16)] and total stress σ_{tot}/σ_0 [the solid red lines; see Eq. (18)] as a function of time for three bond formation times τ_b as indicated in the figure. The red lines include the initial fast Rouse-like relaxation, which is kept the same for all three cases. The curves are shifted by 1 for clarity. The parameters are chosen here as $\tau_e = 0.01$ s, $\tau_\infty = 167$ s, $G_\infty/G_0 = 3$, and $\sigma_{0,e}/\sigma_0 = 3$. This corresponds to $\tau_0 = 500$ s. The time scales τ_e, τ_∞, and τ_0 are indicated by the vertical dashed lines.

We, finally, calculate the time $t_{\max}$ at which the upswing, if any, reaches its maximum. Taking the derivative of Eq. (18) with respect to time, ignoring squares of e^{-t/t_b} because they are negligible at $t = t_{\max}$, and put the result equal to zero, we obtain

$$t_{\max} = \tau_b \ln\left(\frac{\tau_\infty}{\tau_b} + 2\right) + \tau_b \ln\left(\frac{G_\infty - G_0}{G_0}\right). \tag{22}$$

As with the upswing criterion, also $t_{\max}$ depends on the fraction of bonds broken during preshearing.

Numerical results for the cross-link stress in Eq. (16) and the total stress in Eq. (18) are given in Fig. 2 for three different bond formation times τ_b, as indicated in the figure. All other variables are kept constant (and are indicated in the legend of the figure). The dashed blue curves refer to the cross-link stress and the solid red line to the total stress. In Fig. 3, the time dependence of the relative number concentration $c(t)/c_\infty$ of bonds is plotted for the same three cases as in Fig. 2. For $\tau_b = 0.1$ and 10 s, there is a clear maximum in the stress, and indeed the inequality in Eq. (21) applies. As can be seen in Fig. 3, bond formation is completed before the stress is fully relaxed so that the final decay is single exponential with the time constant $\tau_\infty = 167$ s. The stress maximum occurs at later times for slower bond formation,

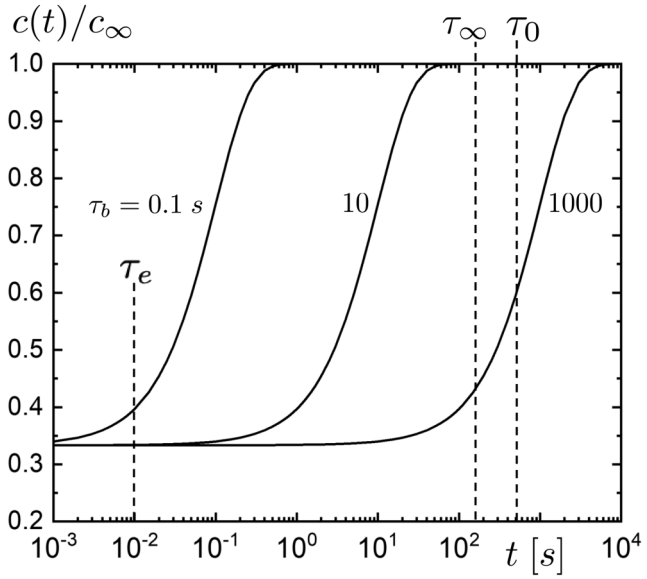

FIG. 3. The time dependence of the number of bonds after the fast Rouse-like relaxation for the three cases in Fig. 2, but for $\tau_b = 0.1$, 10, and 1000 s. The vertical dashed lines indicate the time scales $\tau_e = 0.01$, $\tau_\infty = 167$, and $\tau_0 = 500$ s, corresponding to the values in Fig. 2.

corresponding to larger bond formation times τ_b. Moreover, the maximum becomes less pronounced with increasing τ_b. For sufficiently slow bond formation, the maximum disappears altogether because bond formation cannot compete with stress relaxation so that the decay of the cross-link stress is single exponential with a time constant τ_0, in agreement with Eq. (19), on neglecting the term proportional to $t/\tau_b \ll 1$. The numerical example for $\tau_b = 1000$ s is close to this situation. As can be seen from Figs. 2 and 3, bond formation is not sufficiently advanced during final relaxation to give rise to a maximum in the stress. In this case, $\tau_b/\tau_0 = (G_\infty - G_0)/G_0 = 2$ so that the necessary criterion in Eq. (21) for the occurrence of a maximum is indeed not met.

E. Extracting parameters from experiments

In Sec. III, the various parameters are obtained from a fit of the experimental stress-relaxation curve to Eq. (18). It is, however, also possible to estimate these parameters directly from characteristic features of the experimental data, without performing a complete fit.

The free parameters in a comparison of Eq. (18) with experiments are three time scales (the elastic retraction time τ_e, the bond-formation time τ_b, and the final cross-link relaxation time τ_∞), two initial stresses (the initial Rouse-like stress $\sigma_{0,e}$ and the cross-link stress σ_0, but with the constraint that they should add up to the known initial experimental stress), and the ratio G_∞/G_0 of the shear modulus G_∞ in equilibrium and G_0 right after the elastic retraction. There are thus five independent parameters, four of them determine the Maxwell-like stress in Eq. (16), whose contribution to the total stress is responsible for nonmonotonic stress relaxation.

Estimates of these parameters that can be used as initial values for the data fitting process can be obtained as follows. The two time scales, τ_e and τ_∞, can be readily estimated from the data by plotting them on log-linear scales in the appropriate time regimes. In addition, the initial, Rouse-like relaxation is typically sufficiently fast as compared to the onset of stress upswing so that σ_0 is close to the stress at the minimum of the stress-relaxation curve. The remaining two parameters τ_b and G_∞/G_0 describe the upswing as a result of the relaxation to equilibrium of the perturbed distribution of bonds. To a good approximation, $\tau_b \ln 2$ is the time at which the upswing $(\sigma_{\max} - \sigma_0)/\sigma_0$ reaches half its value for the first time. Here, $\sigma_{\max}$ is the value of the stress at its local maximum for times larger than zero. Moreover, we will show next that $\sigma_{\max}/\sigma_0$ is a good estimate for G_∞/G_0.

To calculate $\sigma_{\max}$, we must substitute $t_{\max}$ from Eq. (22) into the equation for the stress, i.e., Eq. (18), obtaining

$$\begin{aligned}\frac{\sigma_{\max}}{\sigma_0} &= \frac{G_\infty}{G_0}\exp\left\{\frac{\tau_b}{\tau_\infty}\left[\ln\left(\frac{\tau_b}{\tau_\infty}\right) - \ln\left(1+2\frac{\tau_b}{\tau_\infty}\right)\right]\right\} \\ &\quad \times \exp\left\{-\frac{\tau_b}{\tau_\infty}\left[\ln\frac{G_\infty - G_0}{G_\infty} - \frac{G_\infty - G_0}{G_0}\right]\right\} \\ &\approx \frac{G_\infty}{G_0}. \end{aligned} \tag{23}$$

The first relation holds when $\exp\{-t_{\max}/\tau_b\}$ can be neglected, while in the second relation, it is assumed that τ_b/τ_∞ is sufficiently small. In the latter case, we can thus estimate the fraction G_∞/G_0 from $\sigma_{\max}/\sigma_0$ and next τ_b from this result together with the experimental value of $t_{\max}$. The easiest way to do this is to plot the right-hand side of Eq. (22) as a function of τ_b and read off the abscissa at the point where this function reaches the value at the left-hand side.

These remarks hold well in case the three characteristic times $\tau_e \ll \tau_b \ll \tau_\infty$ differ by a few orders of magnitude so that the fits can almost be done in a piece-wise fashion.

III. COMPARISON WITH EXPERIMENTS

A few reasonable requirements on the parameters obtained by adjusting them to describe the data are a consequence of the physical ingredients that are at the basis of our theoretical model. The parameters τ_b and τ_∞, for a given system, must be largely independent of preshear rates (provided there are no pronounced differences in the network structure for different preshear rates). In addition, changes of the various parameters and their relation should allow for a realistic interpretation. It should be kept in mind that we have no access to the system strain γ nor to c_{max} or c_∞, and thus not to absolute values of $c(t)$. This severely hampers the interpretation of variations of system parameters with preshear rates and polymer concentrations.

When discussing the experiments and their representation by our theory, we will not normalize stresses at time zero. In principle, such a normalization is harmless, in that it will have no influence on the quality of the fits or their resulting parameters. On the other hand, normalized stresses may become highly misleading and blur the physical picture. Although the ratios of various contributions to the stress in one stress-time curve remain correct, comparison of different

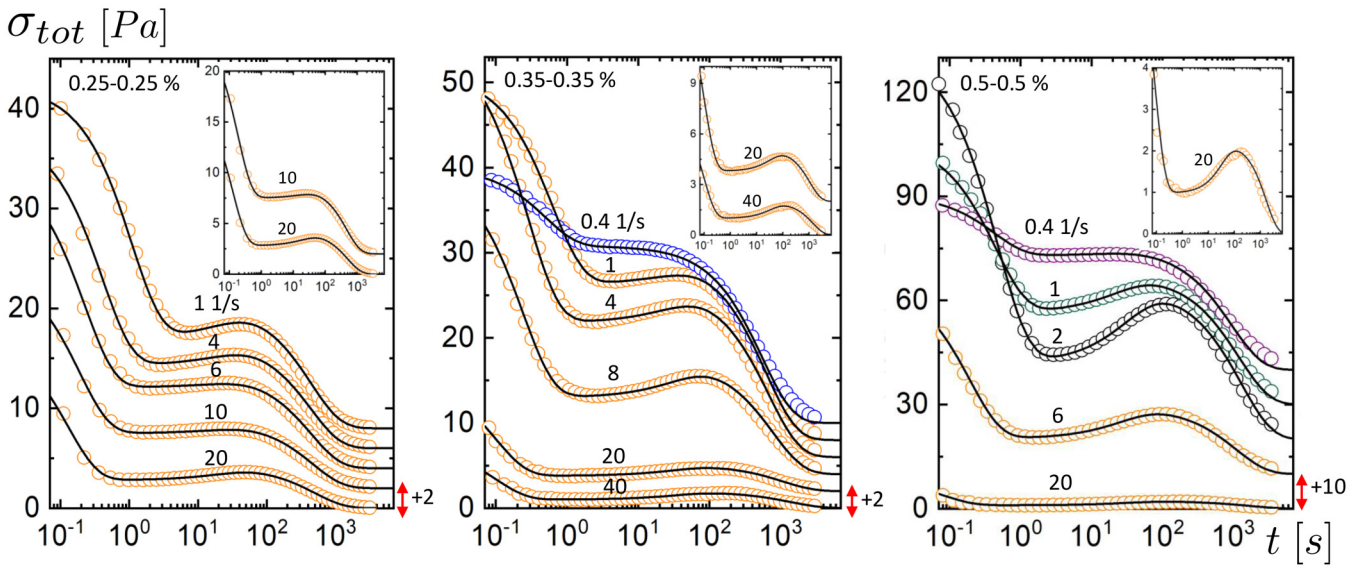

FIG. 4. The time dependence of the total stress for system I, including both the fast initial Rouse-like relaxation and the subsequent relatively slow relaxation, with three different concentrations, increasing from left to right (as indicated in the left top corner of each panel; the two polymers have the same concentration in all the experiments). The preshear rates are indicated just above the corresponding plots. Subsequent data for different preshear rates are shifted for clarity in the vertical direction by an amount that is indicated by the double red arrow on the right bottom of each panel. Also, for clarity, data points for different preshear rates are given in different colors in case the relaxation curves intersect. The solid black lines are fits to Eq. (18). The insets are blow ups for curves that do not exhibit a recognizable maximum on the stress scale in the main panel. Some of the experimental data have previously been published in [2]. Courtesy of Rémi Fournier and Michel Cloitre.

curves becomes difficult. Depending on how the total stress at time zero varies between the different curves, it may happen that the sequence of normalized curves as they are stacked along the vertical axis is the inverse of that for the absolute case. Also, stresses in the time range where the maxima occur and consequently the parameters that describe them may be very similar, while in a normalized presentation stresses in this range appear very different.

A comparison with experiments on three different systems, which we will refer to as systems I, II, and III [2,11–15], is discussed below.

A. Comparison with system I

The first system is a mixture of two polymers dissolved in an aqueous 0.1M NaOH solution at $p\mathrm{H} = 12.5$, with equal polymer weight concentrations of 0.25, 0.35, or 0.50 wt. % [2,11]. One polymer is a partially hydrolyzed polyacrylamide grafted with phenylboronic acid moieties (HPAM-g-PBA), with a molar mass of 780 kg/mol. The other polymer is a fully saponified poly(vinylalcohol), with a molar mass of 125 kg/mol. The phenylboronic acid moeities and the 1, 3 diols form phenylboronic esters, which act as reversible bonds. With an increasing concentration of both polymers, the number of bonds that can form increases. In fact, gels are formed in the semidilute unentangled regime below 2 wt. %.

The experimental stress relaxation curves and their fits to Eq. (18) are given in Fig. 4 for the three concentrations 0.25–0.25, 0.35 − 0.35, and 0.50–0.50 wt. %.

Figure 5 shows the time dependence of the relative bond number concentration c_0/c_∞ for the 0.35–0.35 wt. % sample as obtained from the fits shown as solid lines in Fig. 4 and Eqs. (7) and (15). As expected, the number of bonds right after the preshear has been stopped decreases with increasing preshear rate. More bonds are broken for higher preshear rates.

The initial value $\sigma_{0,tot}$ of the total stress, right after cessation of the preshear, is given in Fig. 6(a) as a function of the preshear rate $\dot{\gamma}_{pre}$. The pronounced maximum is entirely due to a maximum in the initial elastic, Rouse-like stress $\sigma_{0,e}$, which is given in Fig. 6(b). The occurrence of such a maximum is attributed to an increasing (with preshear rate) chain stretching at low preshear rates and a decreasing (with increasing preshear rate) number of stretched unbroken bonds at high preshear rates.

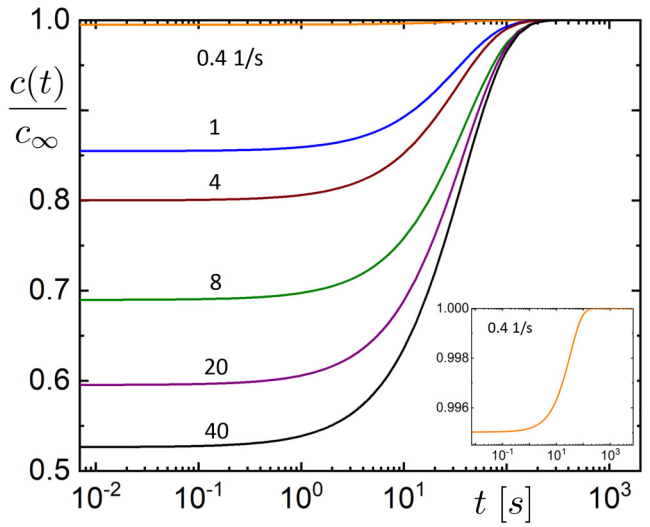

FIG. 5. The time dependence of the number concentration $c(t)$ of bonds, after the fast initial Rouse-like relaxation, relative to its value c_∞ at equilibrium for system I with concentration 0.35%–0.35%. The preshear rates are indicated. The inset is a magnification for the preshear rate 0.4 1/s.

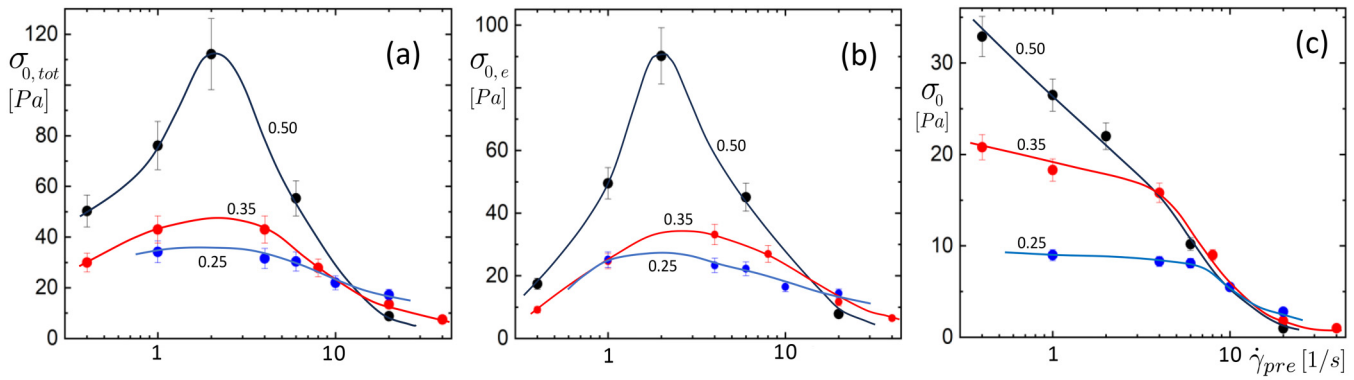

FIG. 6. The parameters for system I as a function of the preshear rate. (a) The total initial stress $\sigma_{0,tot} = \sigma_{0,e} + \sigma_0$, (b) the initial elastic retraction stress $\sigma_{0,e}$, and (c) the initial cross-link stress σ_0 for the three concentrations (as indicated in the figure). The solid lines are guides-to-the-eye. Note that $\sigma_{0,tot}$ includes the fast relaxing elastic Rouse-like stress $\sigma_{0,e}$.

The time-zero cross-link stresses σ_0 are plotted in Fig. 6(c) against the applied preshear rate and are seen to decrease monotonously for all concentrations. At low preshear rates, the values of σ_0 are larger for larger concentrations while the decreases are such that the lower curves join the other ones at preshear rate values about equal to where the maxima occur in Fig. 6(b). From thereon, the various curves continue in one master curve. The results in the low shear rate range can be understood since for systems with larger concentrations more bonds can be broken by preshearing. In the regime where all curves merge, still systems with larger concentrations have more bonds than those with lower concentrations. On the other hand. it becomes increasingly more difficult for the preshear to induce large shear deformations such that apparently $\sigma_0 = G_0 \times \gamma_0$ becomes independent of concentration.

Figure 7(a) shows that the relative number of intact bonds right after cessation of preshear increases with increasing zero-time cross-link stress for all three polymer concentrations. Moreover, for a fixed relative number c_0/c_∞ of intact bonds, the initial cross-link stress increases with increasing polymer concentration. The reason for this is that the cross-link stress is proportional to the *absolute* number of bonds, which increases at constant c_0/c_∞ because c_∞ increases with increasing polymer concentration.

We now discuss relaxation times.

The elastic Rouse-like retraction time τ_e plotted in Fig. 7(b) increases with increasing initial cross-link stress (and hence decreasing preshear rate). The fast elastic retraction, i.e., small τ_e, at small initial network stresses (large preshear rates) is attributed to the existence of only few intact bonds. At larger values of the initial stress, more bonds are present such that, in order for the network to relax, many strands and bonds must move collectively.

The bond formation time $\tau_b = (29 \pm 5)$ s is found to be independent of the preshear rate as expected. In addition to this, it is also independent, within the experimental/fitting error, of the polymer concentration.

The final relaxation time τ_∞ is plotted in Fig. 8 against the rate of preshear. It is seen that τ_∞ increases (apparently linearly) with $\dot{\gamma}_{pre}$ and also increases with polymer concentration. These findings can be rationalized when it is recalled that increasing preshear rates lead to increasing dilution of the cross-link concentration (more bonds are broken) and enhanced network deformation (the network strain increases). So, for larger preshear rates, there are more new bonds to be formed prior to the final stress relaxation, most of which are formed in the then ruling instantaneous nonequilibrium state. As a result, for the larger preshear rates, as the final stress relaxation sets in once all bonds have been re-established, many bonds exist in a nonrelaxed state. During the final, relaxation bonds must break and re-establish in a more

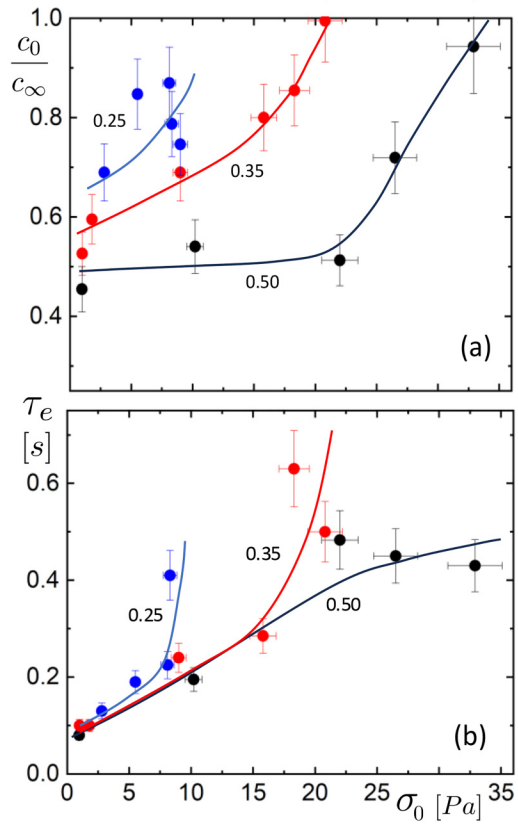

FIG. 7. The relation between (a) the relative amount of unbroken bonds c_0/c_∞ after the initial fast Rouse-like relaxation and (b) the fast elastic Rouse-like retraction time τ_e as a function of the preshear rate $\dot{\gamma}_{pre}$. The solid lines are guides-to-the-eye.

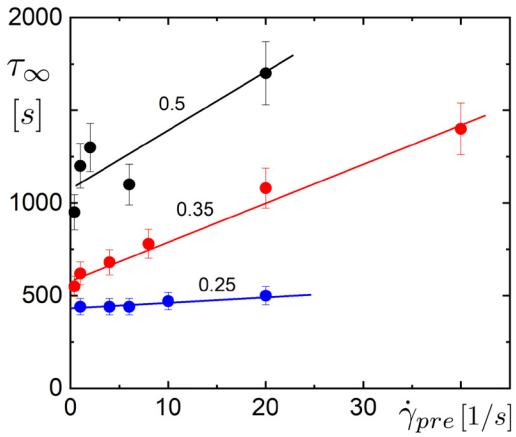

FIG. 8. The final relaxation time τ_∞ as a function of the preshear rate for the three polymer concentration as indicated.

relaxed state. Since re-establishing bonds is relatively fast, breaking bonds is the rate determining process. Hence, with a larger fraction of bonds to be broken, in cases of large preshear rates, the final relaxation stage will require a longer time before the stress has fully relaxed. In addition, once a bond breaks, it will re-form on average in a nonfully equilibrium form, more so for larger network deformation, and needs to be broken again at least once more for full relaxation. Such a multistep relaxation will further delay the final relaxation. In short, τ_∞ increases when more bonds are initially broken and the initial strain increases. The same mechanism also explains why τ_∞ increases with polymer concentration.

As a possible molecular example of this mechanism, we assume that at larger preshear rates, the polymers and/or network strands are aligned, i.e., induce a nonzero nematic order parameter, with a nematic director pointing in the deformation direction of the network. Newly formed bonds locally strengthen the nematic order, which prevents sliding of strands along each other, needed for further decrease in strain. Also, further randomization of the strands (that is, a decrease of the nematic order parameter) needs collective breaking of several bonds along the aligned strands at the same time, which becomes increasingly difficult with increasing nematic order. In case this mechanism is at work, it may be expected that normal stresses, due to residual nematic ordering with a nematic director perpendicular to the shearing direction, are still nonzero after the shear stress has completely relaxed.

The condition for an initial upswing of the stress in Eq. (21) is fulfilled for all three polymer concentrations and those preshear rates where a maximum is seen experimentally. Moreover, for the highest polymer concentration and a preshear rate of 2 1/s, for example, the right-hand side of Eq. (22) for $t_{\max}$ is found from the fitting results of the stress-relaxation in Fig. 4 to be equal to (126 ± 24) s. From the stress-relaxation curve in Fig. 4, we have $t_{\max} = (122 \pm 10)$ s. This verifies the prediction in Eq. (22). Furthermore, from the experimental stress relaxation curve in Fig. 4, we find that $\sigma_{\max}/\sigma_0 = 1.65 \pm 0.15$. From the full Eq. (23), using the fitted parameters, we find that $\sigma_{\max}/\sigma_0 = (1.95 \pm 0.08)*(0.91 \pm 0.01) = 1.77 \pm 0.10$, where the first factor results from G_∞/G_0 and the second factor from the rest of the equation. This agrees well with the experimental value. We note that, using the estimate in the second line in Eq. (23) leads to an error of about 10%.

B. Comparison with system II

The second system is an aqueous solution of a synthetic polymer with a molar mass of 500 kg/mol, with a concentration of 1.35 wt. % in the semidilute region, which is five times the overlap concentration of approximately 0.28 wt.%. 5% of the monomers are side-functionalized with ligands. By adding Fe^{3+} ions, the ligands can be made to mutually bind through the formation of ligand–ion–ligand complexes [13]. Up to three ligands can be bound by a single ion. Two stoichiometric ion/ligand ratios will be discussed below: 1/3 and 1/2. The ratio 1/3 will have relatively more bonds involving three ligands per ion as compared to the 1/2 ratio.

Before discussing the results of our fitting of the stress-upswing of both systems, let us point at an important molecular difference between them. In caricaturization, one may assume that at equilibrium in the 1/2 case, all functionalized groups have found one partner and an ion to form a rather strong ligand–ion–ligand bond; in the 1/3 case, two-third of the groups are formed in this way while the remaining one-third of free ligands join one of these to form ion–$(\text{ligand})_3$. One may speculate that in the first case, there is one dominant strand length, while in the latter case, there are two. Of course, this picture is slightly diluted since not necessarily $c_\infty = c_{\max}$ and bonds continually break and form such that ligands are not permanently bound to the same partners.

Stress relaxation curves for the two ion/ligand ratios are given in Fig. 9, where the solid lines represent the best fits. The two systems clearly behave quite differently. First of all, the time scales associated with bond formation and final relaxation are extremely much larger in the 1/2 case than in the 1/3 case. Moreover, contrary to the 1/2-system, the 1/3-system exhibits very shallow stress maxima, which overlap for all preshear rates to within experimental error (which is about ± 4 Pa). In addition, the initial Rouse-like elastic retraction for the 1/3-system is poorly described by a single-exponential function, contrary to the 1/2-system (except for the highest preshear rate). As a result of this, we can only give rough estimates of parameter values for the 1/3-system.

The nonsingle exponential decay of the initial elastic mode for the 1/3-system is attributed to the existence of two dominant strand lengths, as mentioned above.

Figures 10(a)–10(c) give the initial stresses $\sigma_{0,tot}$, $\sigma_{0,e}$, and σ_0 for the 1/2-system, respectively. The initial total stress $\sigma_{0,tot}$ and the initial elastic stress $\sigma_{0,e}$ increase monotonically with increasing the preshear rate and does not exhibit a maximum at intermediate shear rates as for system I. Contrary to system I, there is apparently not sufficient bond breaking with increasing preshear rate that would give rise to less stretched elastically active chains, which is at the origin of the decrease in the elastic and total stress at larger shear

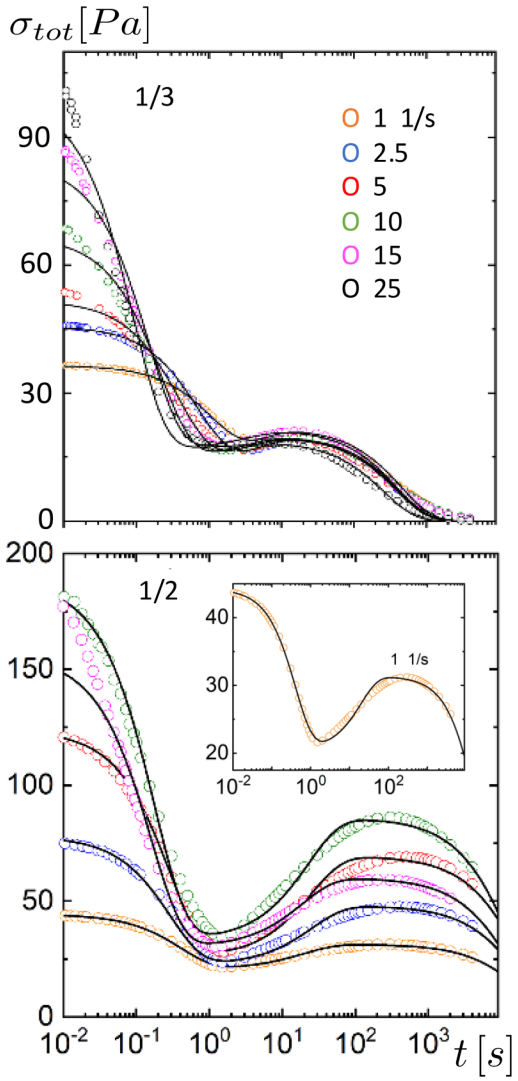

FIG. 9. The time dependence of the total stress for system II with ion/ligand ratios of $1/3$ for the top panel and $1/2$ for the lower panel, including both the fast initial Rouse-like relaxation and the subsequent relatively slow relaxation. The preshear rates are indicated by the same color code in both panels, which are indicated in the upper panel. The solid black lines in both panels are fits to Eq. (18). The inset in the lower panel is a blow up for the curve that does not exhibit a clear recognizable maximum on the stress scale in the main panel. Some of the experimental data have previously been published in [2]. Courtesy of Jan Hendricks and Christian Clasen.

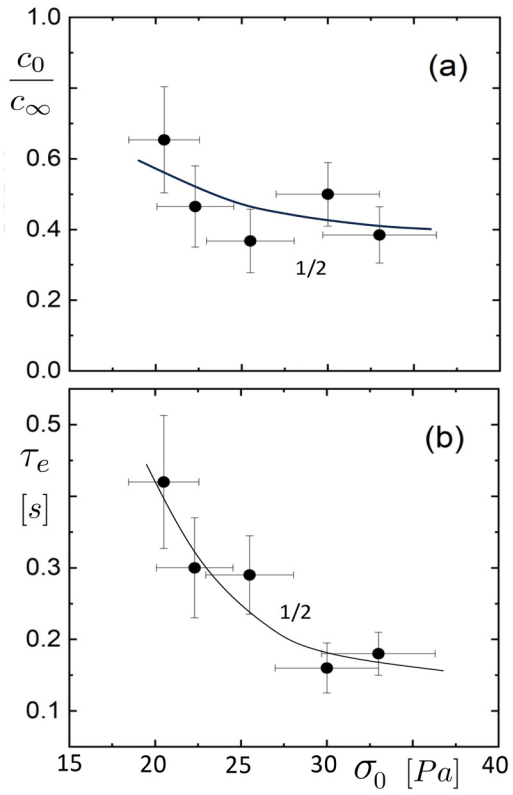

FIG. 11. The relation between the parameters from the fits of the experimental relaxation curves in Fig. 9 (lower panel) for system II for the ion/ligand ratio $1/2$. (a) The initial relative concentration c_0/c_∞ of bonds, after the fast initial Rouse-like relaxation, and (b) the elastic retraction time τ_e as a function of the initial cross-link stress. The solid lines are guides-to-the-eye.

rates. Rough estimates of the initial stresses for the $1/3$-system indicate that all stresses are typically twice smaller than those for the $1/2$-system. This indicates that ion–(ligand)$_2$ bonds are much stronger than ion–(ligand)$_3$ bonds. In view of the comments made earlier concerning the number of both types of bonds in the two systems, the above observations are attributed to strong ion–(ligand)$_2$ bonds and much weaker ion–(ligand)$_3$ bonds.

Figures 11(a) and 11(b) show the initial cross-link concentration and the elastic retraction time for the $1/2$-system as a function of the initial cross-link stress σ_0, respectively.

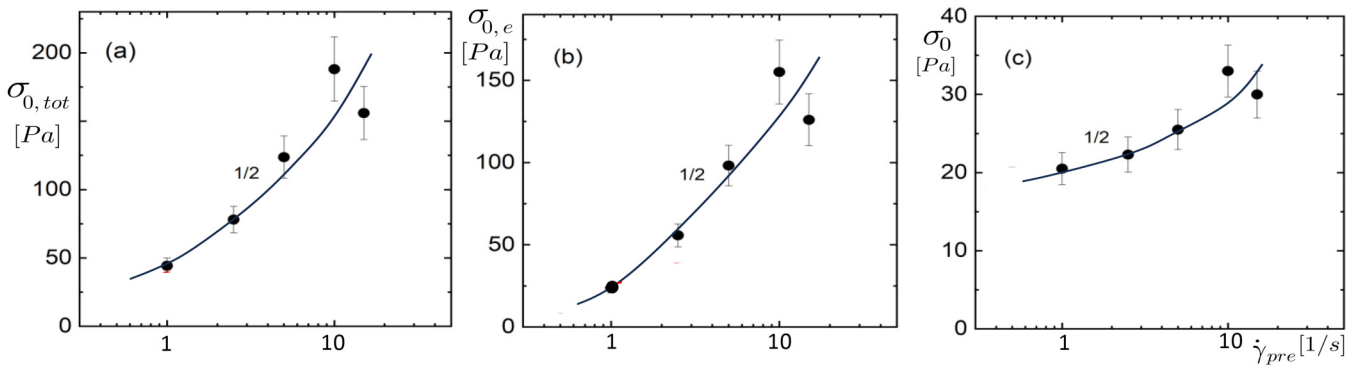

FIG. 10. The parameters for system II with the ion/ligand ratio $1/2$ as a function of the preshear rate. (a) The total initial stress $\sigma_{0,tot} = \sigma_{0,e} + \sigma_0$, (b) the initial elastic retraction stress $\sigma_{0,e}$, and (c) the initial cross-link stress σ_0 for two ion/ligand ratios (as indicated in the figure). The solid lines are guides-to-the-eye. Note that $\sigma_{0,tot}$ includes the fast relaxing elastic Rouse-like stress $\sigma_{0,e}$.

Figure 11(a) reveals that the number of cross-links that survive the preshear is only slightly decreasing with increasing initial cross-link stress (and hence increasing preshear rates). Such a weak dependence is in line with the monotonic increase in the initial cross-link stress with increasing preshear rate in Fig. 10(a): since $\sigma_0 = G_0 \times \gamma_0$, apparently, the increase in the initial strain γ_0 dominates the weak decrease in $G_0 \sim c_0$. The faster elastic relaxation of the elastic stress with decreasing number of bonds [see Figs. 10(a) and 10(b)] is in line with what is found for system I: less remaining bonds leads to faster elastic relaxation as a consequence of the collective nature of elastic relaxation of interacting chains.

We now discuss why τ_∞ is so much larger in the $1/2$-system than in the $1/3$-system. First, as discussed before, the maximum number of ion–$(\text{ligand})_2$ bonds in the $1/3$-system is a factor two-third less than for the $1/2$-system since the total number of ligands is the same in both systems, while the number of ions in the $1/3$-system is a factor $2/3$ less. Since the relative number of bonds that are broken in the two systems is of the same order, the absolute number of broken bonds is, therefore, less in the $1/3$ system. According to the mechanism for final relaxation discussed in the fore-last paragraph for system I, this leads to a faster final stress decay. Second, we speculate that the multistep relaxation process as discussed in the fore-last paragraph for system I is accelerated by the formation of much more intermediate ion–$(\text{ligand})_3$ bonds for the $1/3$-system. Consider an ion–$(\text{ligand})_2$ bond of two polymers a and b, say. A third polymer c can attach to that bond to form an ion–$(\text{ligand})_3$ bond. The two original polymers a and b can now unbind more easily from this weaker ion–$(\text{ligand})_3$ bond as compared to their original ion–$(\text{ligand})_2$ bond. This leads to a new ion–$(\text{ligand})_2$ bond (either a-ion-c or b-ion-c) that is closer to a fully relaxed state. The intermediate formation of ion–$(\text{ligand})_3$ bonds thus "catalysis" the breakage of ion–$(\text{ligand})_2$ bonds, which accelerates the final stress relaxation via the mechanism discussed in the fore-last paragraph for system I.

Finally, we discuss why stress upswings are pronounced in the $1/2$ case while they are weak in the $1/3$ case. For the $1/3$-system, rough estimates are $\tau_\infty \sim 400\,\text{s}$, $\tau_b \sim 3.5\,\text{s}$, $c_0/c_\infty \sim 0.6$, and $\sigma_0 \sim 13\,\text{Pa}$, independent of the preshear rate within experimental/fitting errors. For the $1/2$-system, the bond-formation time is $\tau_b = (22.6 \pm 2.3\,\text{s})$ and $\tau_\infty = (16\,000 \pm 2000)\,\text{s}$, both independent of the preshear rate. From these numbers, it is verified that the criterion in Eq. (21) for the occurrence of upswing is overwhelmingly satisfied for both $1/2$- and $1/3$-systems, but that the initial slope toward the stress maximum in Eq. (20) is about five times larger for the $1/2$-system as compared to the $1/3$-system. Furthermore, the two estimates (22) and (23) in Sec. II E are satisfied for the $1/2$-system.

C. Comparison with system III

The third system with which the theory is compared is an organo gel, consisting of 2, 4-bis (2-ethyl-hexyl-ureido) toluene, commonly abbreviated as EHUT [14,15], dissolved in dodecane. At sufficiently high concentrations, the EHUT bisurea-based monomers self-assemble into supramolecular tubes due to the formation of hydrogen bonds between the urea groups. The data discussed below are obtained in the tube region of the phase diagram at a concentration of $12\,\text{g/dm}^3$. The cross-sectional tube diameter is $\sim 2.6\,\text{nm}$, corresponding to a subassembly of three EHUT monomers [12].

Contrary to the two systems discussed above, the tubes represent "polymers" that can break. More importantly, there are no cross-links that give rise to a network stress, which is instead solely due to entanglements. There is, however, a difference between the supramolecular polymer and common molecular polymers. During preshearing, the supramolecular polymer is partly broken into pieces. After cessation of shear, these pieces grow together again to form the new supramolecular polymer. Because of the strong energetic driving force to form bonds, the newly grown polymers can have entanglement distributions that are totally different from those in conventional polymers. This process may be assumed to give rise to stress upswings when the distribution of entanglements is relaxing toward its common form. Our basic Eqs. (3), (5), (7), and (12) might apply also to such "entangled networks" without cross-links, where the cross-link concentration is replaced by the concentration of entanglements. The justification of the validity of our approach for such entangled networks requires further study and might be based on models like the multichain slip-stick approach [16–19], with the possible addition of polymer-breakage. The comparison of our theory with the experiments for this system should, therefore, be taken with some reservation.

The experimental stress relaxation data for this supramolecular system are given in Fig. 12 for various preshear rates, ranging from 7 to $30\,1/\text{s}$. As can be seen, there are little differences between the stress relaxation curves for the various preshear rates. Within experimental error, the fitting parameters are the same for all preshear rates. In particular, the initial cross-link stress is within the interval $\sigma_0 \in (9.0 \pm 0.4)\,\text{Pa}$, with no systematic variation with the preshear rate. The bond-formation times τ_b are equal to $(4.2 \pm 0.7)\,\text{s}$, while the relaxation times τ_∞ are equal to $(23 \pm 1)\,\text{s}$. Within experimental errors there is no systematic variation of these times with the applied preshear rate. The same holds for the remaining parameters: $\tau_e \in (0.035 \pm 0.008)\,\text{s}$, $c_0/c_\infty \in (0.70 \pm 0.05)$, and $\sigma_{0,e} \in (25 \pm 7)\,\text{Pa}$, again without a systematic variation with the preshear rate.

The experimental data, therefore, do not allow to obtain trends of the various parameters depending on the preshear rate.

An explanation for the insensitivity of various relaxation curves on the preshear rate for this supramolecular system is that essentially full distortion of the network is already achieved for shear rates below the lowest applied preshear rate of 7 1/s.

IV. A NOTE ON GRADIENT SHEAR BANDING OF ASSOCIATIVE POLYMERS

That gradient shear banding is a general feature of associative polymers has been suggested in [20]. In particular, there are strong indications that associative polymer networks

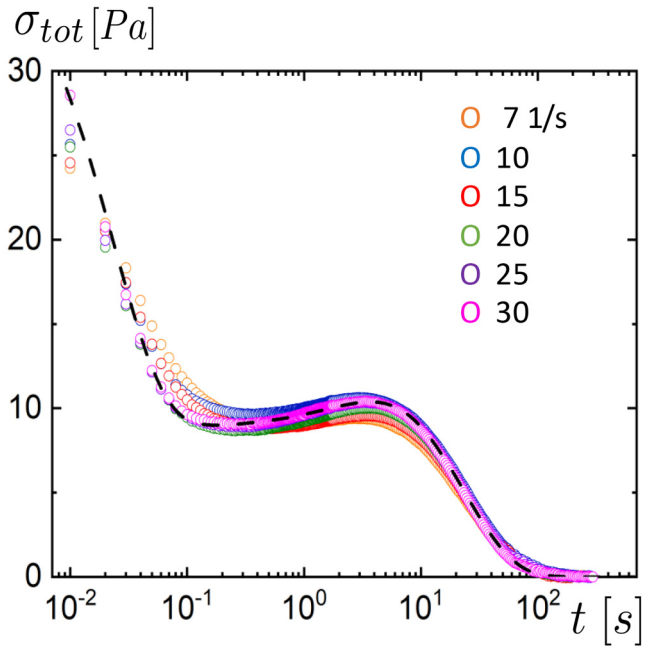

FIG. 12. Experimental stress relaxation curves for system III, including both the fast initial Rouse-like relaxation and the subsequent relatively slow relaxation. Different curves correspond to different preshear rates, which are indicated in the figure. The stress at the time of preshear cessation are, for increasing preshear rates from 7 to 30 1/s, respectively, 28.0, 30.6, 28.9, 31.2, 32.9, and 34.7 Pa. The dashed curve is the fit for a preshear rate of 30 1/s (the magenta data). The experimental data have previously been published in [2]. Courtesy of Ameur Louhichi and Dimitris Vlassopoulos.

with a nonmonotonic stress relaxation exhibit gradient shear banding [Hendricks et al. (personal communication)]. In the stationary state where bands are fully developed, the shear-banded state typically consists of two coexisting regions (the "bands") extending along the gradient direction, each with a different band-internal shear rate. The shear rates within the two bands are (approximately) constant, independent of position. Shear banding occurs under strain-controlled conditions when the stress of a *homogeneously* sheared system, before banding sets in, decreases with increasing shear rate (see, for example, [21] and [22]).

For the present case of associative polymers, the strain γ of the elastic network subjected to an externally imposed shear rate $\dot{\gamma}$ attains a finite value, depending on how fast bonds break and form. That is,

$$\gamma \equiv \gamma(\dot{\gamma}). \tag{24}$$

The stress due to the network's strain can thus be regarded as a function of the applied shear rate. As shown in Appendix C, the total stress of a homogeneously sheared system, with a constant shear rate throughout the system, decreases with increasing shear rate when

$$\frac{d\gamma(\dot{\gamma})}{d\dot{\gamma}} < -\frac{d}{d\dot{\gamma}}[\dot{\gamma}\,\eta(\dot{\gamma})]/\frac{d}{d\gamma}[\gamma\,G(\gamma)], \tag{25}$$

where η is the system's viscosity and, as before, G is the network's shear modulus. The requirement for gradient shear banding of associative polymer networks is thus that the network strain (for a homogeneously sheared network) decreases sufficiently rapidly with the increasing shear rate. Since bond breakage leads to a diminished network strain, a sufficiently rapid increase in bond breaking with increasing shear rate can thus lead to shear banding. In other words, *there should be a sufficient degree of bond breakage on increasing the applied shear rate to render a linear flow profile unstable*.

A van der Waals looplike dependence of the stress on the shear rate is measured as long as the flow profile is linear before shear-banding sets in. Such a van der Waals looplike behavior is found in experiments on associative polymers discussed in Sec. III, even though these experiments extend over large periods of time [Hendricks et al. (personal communication)]. This implies that banding kinetics is very slow, and that for the experiments for which we analyze the nonmonotonic stress relaxation, the flow profile is most probably linear. As a consequence, the polymer and bond number concentrations are uniform, as is assumed from the outset in our generic model. Moreover, even if shear bands would fully develop before cessation of the preshear, our model is still applicable when the differences in the polymer and bond number concentrations within the two bands are not significantly different (simulations in [23] predict limited differences in concentrations).

V. COMPARISON WITH EARLIER THEORIES

Our approach is based on three fundamental equations: the equation of motion (5) for the rate-of-change of the strain, the linear relation (7) between the shear modulus and the concentration of elastically active chains (EACs), and the equation of motion (12) for the number concentration of bonds. Our model is generic in the sense that it also applies to cases where these fundamental equations differ from ours in their details. In such cases, our model generally requires numerical work to obtain the stress. It is out of the scope of the present paper to discuss the vast literature on polymer-network elasticity and the dynamics of associative polymer networks, in relation to the validity of the three fundamental Eqs. (5), (7), and (12). Some of the earlier papers in chronological order are [7,8,24–33], and some of the more recent studies can be found in [5,34–43].

The first experiments where nonmonotonic stress relaxation of associative polymer networks is reported and an attempt to quantitatively describe the time dependence of the stress is presented in [2]. Here, it is argued that nonmonotonic stress decay does not violate the second law of thermodynamics as commonly believed at that time. The second law is not violated due to the significant decrease in the internal energy upon the formation of bonds. An equation of motion for the stress is proposed that is similar to the present Eq. (6). The prefactors of the stress on the right-hand side of that equation of motion in [2] are introduced by intuition and differ from those in the present approach.

The first time the possibility of a nonmonotonic stress relaxation of the shear modulus was mentioned by Joshi [44]. In a subsequent publication [3], prior to the work

discussed above [2], he introduced the classic Maxwell model with a time dependent shear modulus as a possible theoretical framework to describe nonmonotonic stress relaxation. This work has been summarized succinctly and in a clear way in a recent paper by Kumar *et al.* [45], coauthored by Joshi. Our model is in that same spirit.

In order to clarify the relation between our work and that of Joshi, we cannot do better than to point at the differences. In short terms, the most important difference between the two approaches is that Joshi describes the initial decay and the subsequent increase in the stress, while we describe the stress increase and the subsequent final decay to zero. Joshi's model does a good job up to the time when experimentally the stress increase starts to level off again (see cartoon in Fig. 10 in Kumar *et al.* [45]), after which the description is basically aborted. We refrain from describing the initial fast decay and simply model it with the simplest phenomenological equation. This difference in application leads to severe differences in the physical interpretation of the various parameters that appear in the description by means of the mathematical differential equation, the Maxwell model with time dependent shear modulus.

To discuss the difference between the (physical) interpretations of the two models, it is useful to mention that Joshi introduces a parameter $\tau(t)$, which in our notation reads $1/[\mathcal{S}G(t)]$. Joshi's approach is based on the classic Maxwell model, where the system is assumed to consist of a fluid and solid part, with equal contributions to the total stress. In our approach, the fluid part plays no role as flow relaxes on time scales very much smaller than the times scales of interest. Our equation of motion (6) for the cross-link stress is formally identical to that in the classic Maxwell model, but with the inverse of the viscosity η of the fluid part replaced by the bond-snapping parameter $\mathcal{S}$. In that sense, the time scale τ in Joshi's approach is to be interpreted as $\eta/G(t)$. Next, he introduces two phenomenological power laws to describe the time dependence of $\tau(t)$ and $G(t)$, respectively. This provides him with two exponents, q and μ, to achieve a nonmonotonous behavior of the stress. In our application, it is quite natural to define $\gamma(t) = \sigma(t)/G(t)$ and to suggest (differential) equations for $\gamma(t)$ and $G(t)$. This provides us with two parameters, K_+ and K_-, to achieve nonmonotonous behavior of the stress. The precise relation between these two parameters and the directly measurable characteristic times τ_b and τ_∞ is given at the end of Sec. VI.

Quite recently, the same type of nonmonotonic stress relaxation has been observed in shear step-down experiments for carbon-black suspensions [4], for fumed-silica dispersions [5], and in boehmite gels [6]. A thermodynamically consistent microscopic model for such suspensions of aggregating colloidal particles is developed in [46]. The same mechanism for nonmonotonic stress is proposed as for associative polymeric systems, where the temporal increase in the shear modulus is now due to a sufficiently rapid growth of aggregates. The initial elastic stress relaxation for these systems is much slower than for associative polymer networks due to the associated relaxation of the geometry of entire aggregates.

In a recent publication [47], an alternative mechanism for nonmonotonic stress relaxation for soft glassy materials is proposed, being a consequence of gradient shear banding before cessation of the preshear. As already argued in Sec. IV, fully developed shear banding is not a prerequisite for our model, it would not even make a difference.

VI. SUMMARY AND CONCLUSION

A rheological model is proposed to describe the stress-relaxation of associating polymer gels after an extended period of preshearing. The model was applied with great success to three systems for which data have been published in a paper by Hendricks *et al.* [2] and for which additional data were supplied by the authors of that paper. Arguments for the choices made when constructing the model were guided by a coarse molecular picture of these associating polymer systems. At a few points, we made simplifications to obtain greater generality and to allow for a complete analytical solution of the model. The latter allows for explicitly associating model parameters with characteristic points in the data.

The model is based on the fact that immediately after preshearing the system is out of equilibrium, characterized by the fact that the number density of bonds between the functionalized groups has been reduced and that the strands between remaining bonds are strained. It is then assumed that the stress of initially strained strands exhibit a Rouse-like elastic exponential relaxation with a small characteristic time τ_e, as indicated in Fig. 13, essentially without any noticeable change of the number density of bonds. At time scales beyond τ_e, effects of bonds being re-established are dominating the development of the stress. During the initial part of this regime, bonds are re-established with a characteristic time scale of τ_b as indicated in Fig. 13. During this period, the internal strain of the network has not yet relaxed to zero, which implies that the newly formed bonds generate a strained network with an increased number density of bonds. As a result, the stress in the system increases. Finally, after all bonds have been formed, the strain and with it, the stress relaxes at a very slow rate $1/\tau_\infty$ because bonds break and re-form in a slightly relaxed state as indicated in Fig. 13.

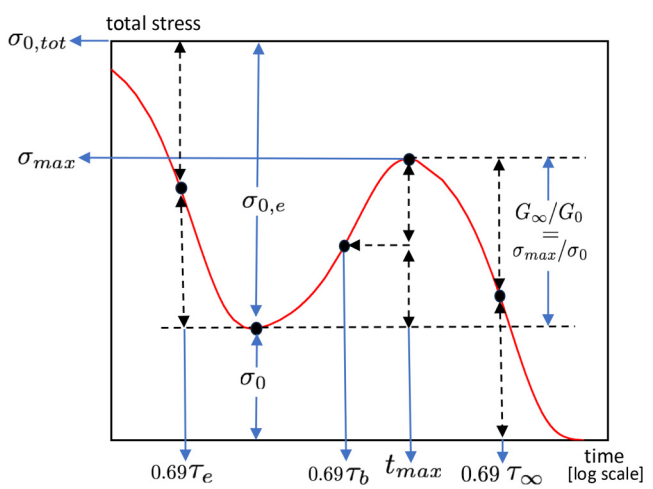

FIG. 13. A schematic, showing how to obtain estimates of the system parameters directly from the experimental stress relaxation curve without performing a detailed fit. The numerical value of $\ln 2 \approx 0.69$ is used.

In addition to the characteristic times just mentioned, there are a few more parameters in figuring our theory all of which are indicated in Fig. 13. The importance of Fig. 13 is that it indicates how all of the parameters in our theory can be estimated from the characteristics of the data. A sharper determination of the parameters of course can be obtained from a full fit of the experimental results.

It is perhaps useful to indicate the relation between the parameters in Fig. 13 and the more basic molecular parameters. We have introduced two reaction rates in our model, the bond-forming rate K_+ and the bond-breaking rate K_-. The sum of the two rates gives the bond-formation time $K_+ + K_- = 1/\tau_b$. As usual with first order reactions, they determine the equilibrium concentration of bonds, c_∞, as given in Eq. (13); $c_{\max}$ in this equation is the maximum number of possible cross-links, which is expressed in terms of c_∞ by Eq. (11). The final relaxation time is related to K_- through $K_- s c_\infty = 1/\tau_\infty$; the only new parameter here is s, the fraction of system strain lost with each breaking bond.

We mention that a strong indication of the quality of the model is given by the fact that the variations of the model parameters with varying systems and/or preshear characteristics can be understood to a large extent by variations of molecular characteristics and network stresses at time zero. In order to predict the latter, the theory must be extended to be applicable to networks under shear.

Clearly, how successful the theory may be, there are several open ends that may need further study. First, we do not differentiate between structure and strain. This was briefly touched when we discussed the results for system I, where it was found that τ_∞ depended on the applied preshear. This is within our theory, in principle, not possible because during the final decay, the cross-link density is equal to its equilibrium value, independent of preshear, and s, K_-, and $\mathcal{A}$ are treated as constants. In order to account for this dependency, we must introduce a structural order parameter besides the strain that is already available. Second, some readers might want to stay closer to the molecular structure of the polymers and make different theories for different systems. This was not our intention here because we wanted to create a framework that can be used for a range of polymer systems. More generally, several of the parameters [in particular, s in the derivation of Eq. (5), f to arrive at Eq. (7), and K_+ and K_- to obtain Eq. (12)] are argued to be independent of γ and c, at least for the associative polymers under consideration in the present work. To specify, such possible dependencies would require a more molecular-based theory, where the structural order parameter mentioned above will certainly come into play. Finally, the main limitation of our theory is that it cannot be used under flowing conditions. The solution of this problem, together with some of the others, may also bring within reach a description of the initial decay, which is now treated *ad hoc*.

ACKNOWLEDGMENTS

The authors are very grateful to Rémi Fournier and Michel Cloitre (ESPCI, France) for providing the experimental data for system I, Jan Hendricks and Christian Clasen (KU Leuven, Belgium) for system II, and Ameur Louhichi and Dimitris Vlassopoulos (FORTH, Greece) for system III.

AUTHOR DECLARATIONS

Conflict of Interest

The authors have no conflicts to disclose.

DATA AVAILABILITY

The data that support the findings of this study are available from the authors of [2] upon reasonable request.

APPENDIX A: BOND-SNAPPING

In the considerations below, we adopt the affine network model where the dangling ends of the network chains are attached to an elastic nonfluctuating polymer backbone that is affinely deformed.

Consider two dangling chains that are attached to the polymer backbone under strain conditions at positions $\mathbf{R}_1$ and $\mathbf{R}_2$. These positions are related to their positions $\mathbf{r}_1$ and $\mathbf{r}_2$ before straining as given in Eq. (B3). The fluctuating positions of the functional groups attached to the dangling ends are denoted as $\mathbf{x}_1$ and $\mathbf{x}_2$, respectively.

We will use coordinates,

$$\begin{aligned} \mathbf{x} &= \mathbf{x}_2 - \mathbf{x}_1 \qquad \mathbf{x}_1 = \mathbf{X} - \mathbf{x}/2, \\ \mathbf{X} &= \frac{\mathbf{x}_2 + \mathbf{x}_1}{2} \qquad \mathbf{x}_2 = \mathbf{X} + \mathbf{x}/2. \end{aligned} \tag{A1}$$

When the distance $x = \mid \mathbf{x}_2 - \mathbf{x}_1 \mid$ between the two functional groups under strain conditions is small enough, they may bind. The total energy may then be written as

$$\begin{aligned} \Phi(\mathbf{x}, \mathbf{X} \mid \gamma) = &-\Delta E_0 \left(1 - \frac{x}{x_b}\right)^2 \Theta(x_b - x) \\ &+ \frac{k}{2} \mid \mathbf{X} - \mathbf{x}/2 - \mathbf{R}_1 \mid^2 + \frac{k}{2} \mid \mathbf{R}_2 - \mathbf{X} - \mathbf{x}/2 \mid^2, \end{aligned} \tag{A2}$$

where the Heaviside function $\Theta(x_b - x)$ ensures that the binding potential only applies when the distance between the two groups is less than the width x_b of the binding potential. The latter is small compared to the size of the macromolecules that makeup the system and so guarantees that the binding well is a narrow well. Furthermore, $\Delta E_0 > 0$ is the binding depth of the potential well of the two functionalized groups. The last two terms on the right-hand side are the contributions due to stretching of the two springlike strands with a spring constant k. When the two groups are bound, the probability for breaking loose is proportional to $e^{-\Delta E/k_B T}$, where

$$\begin{aligned} -\Delta E &= \Phi(\mathbf{0}, \mathbf{X} \mid \gamma) - \Phi(\mathbf{x}_b, \mathbf{X} \mid \gamma) \\ &= -\Delta E_0 + \frac{k}{2} \mathbf{x}_b \cdot (\mathbf{R}_2 - \mathbf{R}_1) + \frac{k}{4} x_b^2, \end{aligned} \tag{A3}$$

with $\mathbf{x}_b = (\mathbf{x}/x) x_b$. Stretching of the chains over distances as small as x_b requires an energy much smaller than the thermal

energy so that the last term in the above result may be neglected in the probability for bond breaking. Both in the nonstrained and the strained state, the chains tend to pull the bonded functional groups in a direction of the chain attachment positions. There is thus a preferred direction of $\mathbf{x}$ along $\mathbf{R}_2 - \mathbf{R}_1$ so that on average,

$$\mathbf{x}_b \cdot (\mathbf{R}_2 - \mathbf{R}_1) \approx x_b \ |\mathbf{R}_2 - \mathbf{R}_1| \,, \tag{A4}$$

up to a factor of order unity. From Eq. (B3), we have

$$\begin{aligned} |\,\mathbf{R}_2 - \mathbf{R}_1\,|^2 = &|\,\mathbf{r}_2 - \mathbf{r}_1\,|^2 \\ &+ 2\gamma\,(\mathbf{r}_{2,x} - \mathbf{r}_{1,x})\,(\mathbf{r}_{2,y} - \mathbf{r}_{1,y}) \\ &+ \gamma^2\,(\mathbf{r}_{2,y} - \mathbf{r}_{1,y})^2, \end{aligned} \tag{A5}$$

where, as before, $\mathbf{r}_{1,2}$ are the position coordinates in the nonstrained state, while x is the straining direction and y is the gradient direction. Expanding the square root of the right-hand side of Eq. (A5) with respect to the last two terms up to order γ^2 and averaging with respect to the nonstrained positions, using that

$$\begin{aligned} \langle(\mathbf{r}_{2,x} - \mathbf{r}_{1,x})\,(\mathbf{r}_{2,y} - \mathbf{r}_{1,y})\rangle &= 0, \\ \langle(\mathbf{r}_{2,y} - \mathbf{r}_{1,y})^2\rangle &= 4\,l_0^2/3, \end{aligned} \tag{A6}$$

with $l_0 = |\,\mathbf{r}_2 - \mathbf{r}_1\,|/2$ the average distance between cross-links in equilibrium, it is found that, to leading order in γ,

$$|\,\mathbf{R}_2 - \mathbf{R}_1\,| = 2\,l_0\left[1 + \frac{1}{15}\,\gamma^2\right]. \tag{A7}$$

The bond-breakage probability R_- is, therefore, again to leading order in the strain,

$$\begin{aligned} R_- &= \nu \exp\{-\beta\,\Delta E\} \\ &= \nu \exp\Big\{-\beta\,(\Delta E_0 - k\,x_b\,l_0)\Big\} \\ &\quad \times \left[1 + \frac{1}{15}\,\beta\,k\,x_b\,l_0\,\gamma^2\right], \end{aligned} \tag{A8}$$

where ν is some attempt frequency. Defining

$$K_- = \nu \exp\Big\{-\beta\,(\Delta E_0 - k\,l_0\,x_b)\Big\}, \tag{A9}$$

we obtain Eq. (4) from the main text.

APPENDIX B: CROSS-LINK DENSITY DEPENDENCE OF THE SHEAR MODULUS FOR GAUSSIAN CHAINS

In our model, cross-links are force bearing elements, while the polymer strands only transmit the forces. We therefore write the stress in the system as

$$\begin{aligned} \sigma_{xy} &= -\frac{1}{V}\sum_i \langle R_{i,x} F_{i,y}\rangle \\ &= -\frac{1}{V}\sum_{i>j} \langle (R_{i,x} - R_{j,x})\,F_{ij,y}\rangle, \end{aligned} \tag{B1}$$

where i and j run over all cross-links and the pointy arrows indicate an average over all configurations compatible with the fixed number of cross-links and their geometrical distribution. $R_{i,x}$ denotes the x-coordinate of cross-link i and $F_{ij,y}$ the y-component of the force exerted on cross-link i by cross-link j. Introducing the Rouse force transmitted by the polymer strands, we get

$$\sigma_{xy} = \frac{1}{V}\sum_i \left\langle \frac{1}{2}\sum_{j\in N_i} (R_{i,x} - R_{j,x})\,\frac{3k_BT}{nb^2}\,(R_{i,y} - R_{j,y}) \right\rangle, \tag{B2}$$

with k_B being the Boltzmann constant, b being the Kuhn-length, and n being the number of Kuhn-lengths per strand; N_i is the set of neighbors of cross-link i that are connected to it via a polymer strand. Letting y be the gradient direction, we have

$$\begin{aligned} R_{i,x} - R_{j,x} &= (r_{i,x} - r_{j,x}) + (r_{i,y} - r_{j,y})\,\gamma, \\ R_{i,y} - R_{j,y} &= (r_{i,y} - r_{j,y}), \end{aligned} \tag{B3}$$

where $r_{i,x}$ is the x-coordinate of particle i in the unsheared state. With these and the fact that the averaging is now over cross-link configurations in the nonsheared state, we get for the stress

$$\sigma_{xy} = \frac{1}{V}\sum_i \frac{3k_BT}{nb^2}\left\langle \frac{1}{2}\sum_{j\in N_i} (r_{i,y} - r_{j,y})^2 \right\rangle \gamma, \tag{B4}$$

where $\langle (r_{i,x} - r_{j,x})(r_{i,y} - r_{j,y})\rangle = 0$ has been used. The shear modulus then reads

$$G = c\,\frac{3k_BT}{nb^2}\left\langle \frac{1}{2}\sum_{j\in N_i} (r_{i,y} - r_{j,y})^2 \right\rangle. \tag{B5}$$

Letting z be the bond-coordination number, we get

$$G = c\,\frac{3k_BT}{nb^2}\,\frac{z}{2}\,\langle (r_{i,y} - r_{j,y})^2\rangle. \tag{B6}$$

With end-functionalized polymers, we may assume that the average distance squared will be independent of the cross-link density, and we arrive at the law introduced in the main text. In case the cross-links are randomly distributed along the polymer-backbone, we assume that $\langle (r_{i,y} - r_{j,y})^2\rangle = l_0^2/3$ is proportional to $c^{-2/3}$ and n is proportional to c^{-1}, which finally yields $G \propto c^{4/3}$. The scaling of the shear modulus with the bond number concentration will be different for non-ideal Rouse chains, where the force is not proportional to the chain extension. What is essential is that the shear modulus is an increasing function of the number of bonds. For this

reason, and to keep the equations tractable, we ignore the fact that there may be deviations from a linear dependence of the shear modulus with the number of bonds, and stick to $G = \mathcal{A}c$. Note that this underestimates the degree of nonmonotonic stress relaxation as compared to the $\sim c^{4/3}$ dependence.

APPENDIX C: SHEAR BANDING OF ASSOCIATIVE POLYMER NETWORKS

For the associative polymer networks subjected to an externally applied shear rate $\dot{\gamma}$, the total stress is equal to

$$\sigma(\dot{\gamma}) = \sigma_f(\dot{\gamma}) + \sigma_s(\dot{\gamma}), \tag{C1}$$

where $\sigma_f(\dot{\gamma})$ is the stress of the purely viscous, fluid part of the system (free polymers and possibly solvent), and $\sigma_s(\dot{\gamma})$ is the stress of the solid part of the system, that is, the network's cross-link stress,

$$\begin{aligned} \sigma_f(\dot{\gamma}) &= \dot{\gamma}\,\eta(\dot{\gamma}), \\ \sigma_s(\dot{\gamma}) &= \gamma(\dot{\gamma})\,G(\gamma(\dot{\gamma})), \end{aligned} \tag{C2}$$

where η is the viscosity of the fluid part and, as before, G is the shear modulus of the network. Here, Eq. (24) for the shear-rate dependence of the network strain has been substituted.

Consider a two-plate geometry with y being the distance from the lower stationary plate, which is the gradient direction. For an inhomogeneous flow profile that evolves with time, the shear rate (and hence, the network's strain) varies with position y and is a function of time. Assuming low Reynolds numbers, the Navier–Stokes equation for the flow velocity u reduces to

$$\rho\,\frac{\partial u(y,t)}{\partial t} = \frac{\partial}{\partial y}[\sigma_f(\dot{\gamma}(y),t) + \sigma_s(\dot{\gamma}(y),t)], \tag{C3}$$

with ρ being the mass density of the system, which can be assumed independent of the position.

To assess the condition under which a linear flow profile, with a position-independent shear rate $\dot{\gamma}$, becomes unstable proceeds just like for purely viscous systems as follows. Consider a small sinusoidal perturbation with wavelength $\lambda = 2\pi/k$ of the linear velocity profile $u(y,t) = \dot{\gamma}\,y + \epsilon(t)\sin\{ky\}$, with $\epsilon(t)$ being a relatively small contribution to the flow velocity so that $\sigma(y,t) = \sigma(\dot{\gamma}) + [d\sigma(\dot{\gamma})/d\dot{\gamma}]\,\epsilon(t)\,k\cos\{ky\}$. Substitution into Eq. (C3) and linearization with respect to $\epsilon(t)$ leads to

$$\epsilon(t) \sim \exp\left\{-\frac{1}{\rho}\,\frac{d\sigma(\dot{\gamma})}{d\dot{\gamma}}\,k^2\,t\right\}. \tag{C4}$$

A linear flow profile with shear rate $\dot{\gamma}$ is thus absolutely unstable when

$$\frac{d\sigma(\dot{\gamma})}{d\dot{\gamma}} = \frac{d}{d\dot{\gamma}}\left[\sigma_f(\dot{\gamma}) + \sigma_s(\dot{\gamma})\right] < 0. \tag{C5}$$

Contrary to gradient banding of purely viscous systems, in the present case, we have $d\sigma_f(\dot{\gamma})/d\dot{\gamma} > 0$. Substitution of Eq. (C2) now leads to the following criterion for gradient shear banding of associative polymer networks:

$$\frac{d}{d\gamma}[\gamma\,G(\gamma)] \times \frac{d\gamma(\dot{\gamma})}{d\dot{\gamma}} < -\frac{d}{d\dot{\gamma}}\,[\dot{\gamma}\,\eta(\dot{\gamma})], \tag{C6}$$

which immediately leads to Eq. (25).

As is well-known, additional higher order spatial gradients of the flow field should be added to the right-hand side of Eq. (C3) in order to prevent the unphysical arbitrary rapid increase in small wavelength perturbations as predicted in Eq. (C4) and to account for the large spatial gradients of the fluid flow velocity within the interface between the two bands (see, for example, [21] and [22]).

REFERENCES

[1] Louhichi, A., Supramolecular assemblies and networks: Interactions, viscoelasticity and flow, Ph.D. dissertation, University of Crete, Crete, 2017.

[2] Hendricks, J., A. Louhichi, V. Metri, R. Fournier, N. Reddy, L. Bouteiller, M. Cloitre, C. Clasen, D. Vlassopoulos, and W. J. Briels, "Nonmonotonic stress relaxation after cessation of steady shear flow in supramolecular assemblies," Phys. Rev. Lett. **123**, 218003 (2019).

[3] Joshi, Y. M., "Thixotropy, nonmonotonic stress relaxation, and the second law of thermodynamics," J. Rheol. **66**, 111–123 (2022).

[4] Wang, Y., and R. H. Ewoldt, "New insights on carbon black suspension rheology—Anisotropic thixotropy and antithixotropy," J. Rheol. **66**, 937–953 (2022).

[5] Choi, J., M. Armstrong, and S. A. Rogers, "The role of elasticity in thixotropy: Transient elastic stress during stepwise reduction in shear rate," Phys. Fluids **33**, 033112 (2021).

[6] Sudreau, I., M. Auxois, M. Servel, É. Lécolier, S. Manneville, and T. Divoux, "Residual stresses and shear-induced overaging in boehmite gels," Phys. Rev. Mater. **6**, L042601 (2022).

[7] Tanaka, F., and S. F. Edwards, "Viscoelastic properties of physically crosslinked networks. 1. Transient network theory," Macromolecules **25**, 1516–1523 (1992).

[8] Tanaka, F., and S. F. Edwards, "Viscoelastic properties of physically crosslinked networks," J. Non-Newtonian Fluid Mech. **43**, 247–271 (1992).

[9] Larson, R. G., "Constitutive equations for thixotropic fluids," J. Rheol. **59**, 595–611 (2015).

[10] Mujumdar, A., A. N. Beris, and A. B. Metzner, "Transient phenomena in thixotropic systems," J. Non-Newtonian Fluid Mech. **102**, 157–178 (2002).

[11] Fournier, R., Ph.D. thesis, Université Pierre et Marie Curie, Paris, 2019.

[12] Bouteiller, L., O. Colombani, F. Lortie, and P. Terech, "Thickness transition of a rigid supramolecular polymer," J. Am. Chem. Soc. **127**, 8893–8898 (2005).

[13] Brassinne, J., A. Cadix, J. Wilson, and E. van Ruymbeke, "Dissociating sticker dynamics from chain relaxation in supramolecular polymer networks—The importance of free partner!," J. Rheol. **61**, 1123–1134 (2017).

[14] Ducouret, G., C. Chassenieux, S. Martins, F. Lequeux, and L. Bouteiller, "Rheological characterisation of bis-urea based viscoelastic solutions in an apolar solvent," J. Colloid Interface Sci. **310**, 624–629 (2007).

[15] Shikata, T., T. Nishida, B. Isare, M. Linares, R. Lazzaroni, and L. Bouteiller, "Structure and dynamics of a bisurea-based

supramolecular polymer in *n*-dodecane," J. Phys. Chem. B **112**, 8459–8465 (2008).
[16] Masubuchi, Y., J. I. Takimoto, K. Koyama, G. Ianniruberto, G. Marrucci, and F. Greco, "Brownian simulations of a network of reptating primitive chains," J. Chem. Phys. **115**, 4387–4394 (2001).
[17] Likhtman, A. E., "Single-chain slip-link model of entangled polymers: Simultaneous description of neutron spin-echo, rheology, and diffusion," Macromolecules **38**, 6128–6139 (2005).
[18] Ramírez-Hernández, A., B. L. Peters, M. Andreev, J. D. Schieber, and J. J. de Pablo, "A multichain polymer slip-spring model with fluctuating number of entanglements for linear and nonlinear rheology," J. Chem. Phys. **143**, 243147 (2015).
[19] Masubuchi, Y., and T. Uneyama, "Retardation of the reaction kinetics of polymers due to entanglement in the post-gel stage in multi-chain slip-spring simulations," Soft Matter **15**, 5109–5115 (2019).
[20] Sprakel, J., E. Spruijt, M. A. Cohen Stuart, N. A. M. Besseling, M. P. Lettinga, and J. van der Gucht, "Shear banding and rheochaos in associative polymer networks," Soft Matter **4**, 1696–1705 (2008).
[21] Dhont, J. K. G., "A constitutive relation describing the shear-banding transition," Phys. Rev. E **60**, 4534–4544 (1999).
[22] Lu, C.-Y. D., P. D. Olmsted, and R. C. Ball, "Effects of non-local stress on the determination of shear banding flow," Phys. Rev. Lett. **84**, 642–645 (2000).
[23] Sprakel, J., E. Spruijt, J. van der Gucht, J. T. Padding, and W. J. Briels, "Failure-mode transition in transient polymer networks with particle-based simulations," Soft Matter **5**, 4748–4756 (2009).
[24] Green, M. S., and A. V. Tobolsky, "A new approach to the theory of relaxing polymeric media," J. Chem. Phys. **14**, 80–92 (1946).
[25] Flory, P. J., *Principles of Polymer Chemistry* (Cornell University, Ithaca, 1953), Chap. XI.
[26] James, H. M., and E. Guth, "Statistical thermodynamics of rubber elasticity," J. Chem. Phys. **21**, 1039–1049 (1953).
[27] Flory, P. J., "Elasticity of polymer networks cross-limked in states of strain," Trans. Faraday Soc. **56**, 722–743 (1960).
[28] Flory, P. J., "Network topology and the theory of rubber elasticity," Br. Polym. J. **17**, 96–102 (1985).
[29] Baxandall, L. G., and S. F. Edwards, "Deformation-dependent properties of polymer networks constructed by addition of cross-links under strain," Macromolecules **21**, 1763–1772 (1988).
[30] Duering, E. R., K. Kremer, and G. S. Grest, "Structure and relaxation of end-linked polymer networks," J. Chem. Phys. **101**, 8169–8192 (1994).
[31] Khalatur, P. G., A. R. Khokhlov, and D. A. Mologin, "Simulation of self-associating polymer systems. I. Shear-induced structural changes," J. Chem. Phys. **109**, 9602–9613 (1998).
[32] Khalatur, P. G., A. R. Khokhlov, and D. A. Mologin, "Simulation of self-associating polymer systems. II. Rheological properties," J. Chem. Phys. **109**, 9614–9622 (1998).
[33] Tam, K. C., R. D. Jenkins, M. A. Winnik, and D. R. Bassett, "A structural model of hydrophobically modified urethane-ethoxylate (HEUR) associative polymers in shear flows," Macromolecules **31**, 4149–4159 (1998).
[34] Rubinstein, M., and S. Panyukov, "Elasticity of polymer networks," Macromolecules **35**, 6670–6686 (2002).
[35] Goldhirsch, I., and C. Goldenberg, "On the microscopic foundations of elasticity," Eur. Phys. J. E **9**, 245–251 (2002).
[36] Buitenhuis, J., and M. Pönitsch, "Negative thixotropy of polymer solutions. 1. A model explaining time-dependent viscosity," Colloid Polym. Sci. **281**, 253–259 (2003).
[37] *Physical Properties of Polymers Handbook*, edited by J. E. Mark (Springer, 2007), Vol. 1076.
[38] Zhong, M., R. Wang, K. Kawamoto, B. D. Olsen, and J. A. Johnson, "Quantifying the impact of molecular defects on polymer network elasticity," Science **353**, 1264–1268 (2016).
[39] Lin, T.-S., R. Wang, J. A. Johnson, and B. D. Olsen, "Revisiting the elasticity theory for real Gaussian phantom networks," Macromolecules **52**, 1685–1694 (2019).
[40] Gula, I. A., H. A. Karimi-Varzaneh, and C. Svaneborg, "Computational study of cross-link and entanglement contributions to the elastic properties of model PDMS networks," Macromolecules **53**, 6907–6927 (2020).
[41] Jiang, N., H. Zhang, P. Tang, and Y. Yang, "Linear viscoelasticity of associative polymers: Sticky Rouse model and the role of bridges," Macromolecules **53**, 3438–3451 (2020).
[42] Sorichetti, V., A. Ninarello, J. M. Ruiz-Franco, V. Hugouvieux, W. Kob, E. Zaccarelli, and L. Rovigatti, "Effect of chain polydispersity on the elasticity of disordered polymer networks," Macromolecules **54**, 3769–3779 (2021).
[43] Wagner, R. J., E. Hobbs, and F. J. Vernerey, "A network model of transient polymers: Exploring the micromechanics of nonlinear viscoelasticity," Soft Matter **17**, 8742–8757 (2021).
[44] Joshi, Y. M., "A model for aging under deformation field, residual stresses and strains in soft glassy materials," Soft Matter **11**, 3198–3214 (2015).
[45] Kumar, V., G. H. McKinley, and Y. M. Joshi, "Hyperaging and stress build up in soft colloidal gels," J. Rheol. **69**, 855–871 (2025).
[46] Jariwala, S., N. J. Wagner, and A. N. Beris, "A thermodynamically consistent, microscopically-based, model of the rheology of aggregating particles suspensions," Entropy **24**, 717–745 (2022).
[47] Ward, V. K., and S. M. Fielding, "Shear banding as a cause of nonmonotonic stress relaxation after flow cessation," Phys. Rev. Mater. **9**, L022601 (2025).